

# Photometric and spectroscopic study of the intermediate-age open cluster NGC 2355 <sup>†</sup>

P. Donati<sup>1,2</sup>, A. Bragaglia<sup>1</sup>, E. Carretta<sup>1</sup>, V. D’Orazi<sup>3,4,5</sup>, M. Tosi<sup>1</sup>, F. Cusano<sup>1</sup>, R. Carini<sup>6</sup>

<sup>1</sup>INAF-Osservatorio Astronomico di Bologna, via Ranzani 1, I-40127 Bologna, Italy

<sup>2</sup>Dipartimento di Fisica e Astronomia, via Ranzani 1, I-40127 Bologna, Italy

<sup>3</sup>INAF-Osservatorio Astronomico di Padova, vicolo Osservatorio 5, I-35122 Padova, Italy

<sup>4</sup>Department of Physics and Astronomy, Macquarie University, Sydney, NSW 2109, Australia

<sup>5</sup>Monash Centre for Astrophysics, School of Physics and Astronomy, Monash University, Melbourne, VIC 3800, Australia

<sup>6</sup>INAF-Osservatorio Astronomico di Roma, via Frascati 33, I-00078, Monte Porzio Catone, Italy

24 August 2015

## ABSTRACT

In this paper we analyse the evolutionary status and properties of the old open cluster NGC 2355, located in the Galactic anticentre direction, as a part of the long term programme BOCCE. NGC 2355 was observed with LBC@LBT using the Bessel  $B$ ,  $V$ , and  $I_c$  filters. The cluster parameters have been obtained using the synthetic colour-magnitude diagram (CMD) method, as done in other papers of this series. Additional spectroscopic observations with FIES@NOT of three giant stars were used to determine the chemical properties of the cluster. Our analysis shows that NGC 2355 has metallicity slightly less than solar, with  $[\text{Fe}/\text{H}] = -0.06$  dex, age between 0.8 and 1 Gyr, reddening  $E(B-V)$  in the range 0.14 and 0.19 mag, and distance modulus  $(m-M)_0$  of about 11 mag. We also investigated the abundances of O, Na, Al,  $\alpha$ , iron-peak, and neutron capture elements, showing that NGC 2355 falls within the abundance distribution of similar clusters (same age and metallicity). The Galactocentric distance of NGC 2355 places it at the border between two regimes of metallicity distribution; this makes it an important cluster for the study of the chemical properties and evolution of the disc.

**Key words:** Hertzsprung-Russel and colour-magnitude diagrams, Galaxy: disc, open clusters and associations: general, open clusters and associations: individual: NGC 2355.

## 1 INTRODUCTION

This paper is part of the BOCCE (Bologna Open Clusters Chemical Evolution) project, described in detail by Bragaglia & Tosi (2006). BOCCE aims to precisely and homogeneously derive the fundamental properties of a large, significant sample of open clusters (OCs), which are among the best tracers of the Galactic disc properties (e.g., Friel 1995). We have already analysed photometric data for 35 OCs (see Donati et al. 2014a, for updated references), by comparing observed and synthetic colour-magnitude diagrams (CMDs, see Tosi et al. 1991; Bragaglia & Tosi 2006) and producing age, distance, reddening, and approximate metallicity on a homogenous scale. Metallicity and detailed chemical abundances based on high-resolution spectroscopy are instead available for about one third of the sample, see e.g. Carretta, Bragaglia, & Gratton (2007), and Andreuzzi et al. (2011) for a discussion on the use of OCs to ascertain the metallicity distribution in the disc.

<sup>†</sup> Based on observations collected at the Large Binocular Telescope (LBT) and the Nordic Optical Telescope (NOT). The LBT is an international collaboration among institutions in the United States, Italy and Germany. LBT Corporation partners are: The University of Arizona on behalf of the Arizona University system; Istituto Nazionale di Astrofisica, Italy; LBT Beteiligungs-gesellschaft, Germany, representing the Max-Planck Society, the Astrophysical Institute Potsdam, and Heidelberg University; The Ohio State University, and The Research Corporation, on behalf of The University of Notre Dame, University of Minnesota and University of Virginia. The NOT is operated by the Nordic Optical Telescope Scientific Association at the Observatorio del Roque de los Muchachos, La Palma, Spain, of the Instituto de Astrofisica de Canarias.

We present here a photometric and spectroscopic analysis of NGC 2355, an intermediate-age OC located towards the Galactic anticentre ( $l = 203.390$  deg;  $b = 11.803$  deg,

We present here a photometric and spectroscopic analysis of NGC 2355, an intermediate-age OC located towards the Galactic anticentre ( $l = 203.390$  deg;  $b = 11.803$  deg,

**Table 1.** Properties of NGC 2355 in literature sources. If not given in the original paper,  $(m - M)_0$  was computed from  $(m - M)_V$  and  $E(B - V)$ , or from the distance from the Sun.

| Paper   | tel./instr. | FoV/stars            | phot/spec   | age (Gyr)   | $(m - M)_0$ | $E(B - V)$ | [Fe/H] | Notes        |
|---|-------------|----------------------|-------------|-------------|-------------|------------|--------|--------------|
| Kaluzny&Mazur 1991<br>Ann et al. 1999<br>Oliveira et al. 2013 | 0.9m KPNO   | 6.6' $\times$ 6.6'   | <i>UBV</i>  | “Praesepse” | 11.73       | 0.12       | +0.13  |              |
|   | 1.8m BOAO   | 11.8' $\times$ 11.8' | <i>UBVI</i> | 1           | 11.4        | 0.25       | -0.32  | Padova isoc. |
|   |             |                      |             | 0.8         | 11.45       | 0.22       | -0.23  | Using KM91   |
|   |             |                      |             | 0.9         | 10.88       | 0.32       | -0.32  | Using A99    |
| Soubiran et al. 2000  | ELODIE      | 24 stars             | R=42000     | 1           | 11.06       | 0.16       | -0.07  | 17 members   |
| Jacobson et al. 2011  | Hydra       | 12 stars             | R=18000     |             |             |            | -0.08  | 6 members    |

Dias et al. 2002). The cluster has been targeted because of its location in the outer disc ( $R_{GC} \gtrsim 10$  kpc), close to the point where the metallicity distribution seems to flatten, and where only a few OCs have been studied so far. Furthermore, its stars are bright enough to be easily observed with high-resolution spectroscopy.

There are only two previous sources of visual CCD photometry for NGC 2355, both acquired at relatively small telescopes (KPNO and BOAO). Kaluzny & Mazur (1991) obtained *UBV* data, while Ann et al. (1999) presented *UBVI* data; these data have also been reanalysed by others (see Table 1). High-resolution spectra have been obtained by Soubiran, Odenkirchen, & Le Campion (2000), by Jacobson, Pilachowski, & Friel (2011b), and by Jacobson & Friel (2013) to derive metallicity, and by Mermilliod, Mayor, & Udry (2008) addressing radial velocities. These studies are described below (Sect. 3.4). Table 1 presents a summary of the properties derived in literature; while all these authors agree on an intermediate age, a moderate reddening, and a subsolar metallicity (with one exception), an agreement on the specific values has not been reached yet. In the present paper we analyse *BVI* photometric data obtained at the Large Binocular Telescope (LBT) and spectra obtained with the Nordic Optical Telescope (NOT; see Sec. 2 and 3 for a description of data acquisition and reduction), derive detailed abundances (Sec. 3), the cluster age, distance, and reddening using synthetic CMDs (Sec. 4). Discussion and summary are presented in Secs. 5, and 6.

## 2 PHOTOMETRY

### 2.1 Observation and reduction

The cluster was observed as part of the BOCCE program using LBC (Large Binocular Camera) mounted at LBT on Mount Graham (AZ, USA); we refer the reader to Cignoni et al. (2011) and Donati et al. (2014a) for further details. All data were acquired during one night (Feb. 22, 2012), with seeing of about 1.6'' and using the Johnson-Cousins filters (*B* on LBC-Blue and *V, I* on LBC-Red). The log of the observations is given in Table 2. In Fig. 1 we show the field of view of LBC@LBT and highlight the spectroscopic targets.

The raw LBC images were trimmed and corrected for bias and flat-field, using the pipeline developed for LBC image pre-reduction by the Large Survey Center (LSC) team

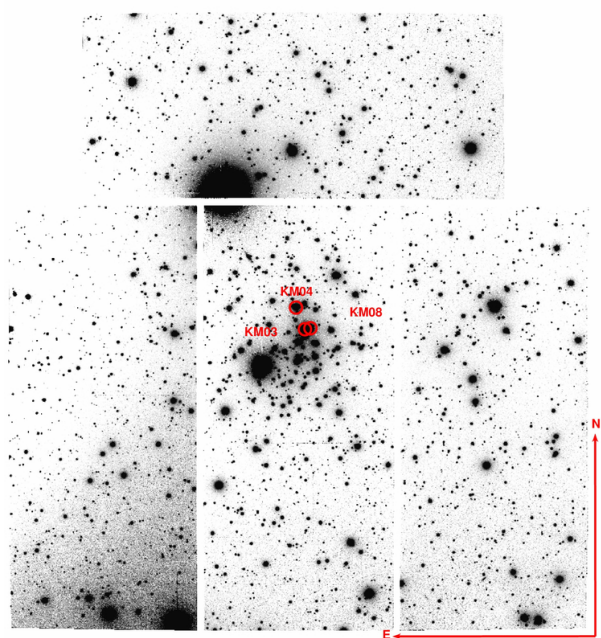


**Figure 1.** The field observed with LBC, corresponding to about  $22 \times 25$  arcmin $^2$ . The red circles indicate the spectroscopic targets. The image is a composition of the CCD mosaic of the instrument obtained in the *V*-BESSEL filter. North is up and East is left.

**Table 2.** Log of LBT and NOT observations.

| Instr. | UT Date     | exp.time (s)   | Note               |
|--------|-------------|--|--------------------|
| LBC    | 2012 Feb 22 | <i>B</i> : $2 \times 1.2$ , $3 \times 5.3$ , $2 \times 90.3$ | seeing 1.5''-1.9'' |
|        |             | <i>V</i> : $2 \times 1.2$ , $3 \times 5.3$ , $3 \times 60.3$ | seeing 1.3''-1.9'' |
|        |             | <i>I</i> : $2 \times 1.2$ , $5.3$ , $2 \times 60.3$          | seeing 1.1''-1.7'' |
| FIES   | 2014 Jan 25 | $3 \times 1800$  | star 201728 (817)  |
|        | 2014 Mar 12 | $3 \times 2100$  | star 201729 (536)  |
|        | 2015 Jan 05 | $3 \times 2100$  | star 201735 (587)  |

at the Rome Astronomical Observatory.<sup>1</sup> The stars were detected independently on each *B*, *V* and *I* image and their photometry performed using the point spread function (PSF)-fitting code DAOPHOTII/ALLSTAR (Stetson 1987, 1994).

We used the error-weighted average of the independent

<sup>1</sup> LSC website: <http://lsc.ox-roma.inaf.it/>

**Table 3.** Completeness of our photometry (in percentage).

| mag  | <i>B</i> | <i>V</i> | <i>I</i> |
|------|----------|----------|----------|
| 15.0 |          | 100 ± 1  |          |
| 15.5 | 100 ± 1  | 97 ± 2   | 100 ± 1  |
| 16.0 | 97 ± 2   | 97 ± 1   | 95 ± 1   |
| 16.5 | 97 ± 1   | 97 ± 1   | 95 ± 1   |
| 17.0 | 98 ± 1   | 98 ± 1   | 94 ± 1   |
| 17.5 | 97 ± 1   | 97 ± 1   | 92 ± 1   |
| 18.0 | 98 ± 1   | 96 ± 1   | 90 ± 1   |
| 18.5 | 97 ± 1   | 95 ± 1   | 84 ± 1   |
| 19.0 | 96 ± 1   | 94 ± 1   | 70 ± 1   |
| 19.5 | 95 ± 1   | 93 ± 1   | 27 ± 1   |
| 20.0 | 95 ± 1   | 91 ± 1   | 3 ± 4    |
| 20.5 | 93 ± 1   | 86 ± 1   |          |
| 21.0 | 93 ± 1   | 76 ± 1   |          |
| 21.5 | 90 ± 1   | 49 ± 1   |          |
| 22.0 | 88 ± 1   | 16 ± 2   |          |
| 22.5 | 82 ± 1   | 2 ± 5    |          |
| 23.0 | 70 ± 1   |          |          |
| 23.5 | 41 ± 1   |          |          |
| 24.0 | 11 ± 2   |          |          |
| 24.5 | 1 ± 7    |          |          |

measurements obtained from the various images as the final value of the instrumental magnitudes. The transformation of instrumental positions (in pixels) to J2000 celestial coordinates was done<sup>2</sup> using, for each chip, about 700 stars from the Sloan Digitized Sky Survey (SDSS, see [www.sdss.org](http://www.sdss.org)) catalogue. The rms scatter of the solution was about 0.1 arcsec in both RA and Dec. We derived the completeness level of the photometry by means of extensive artificial stars experiments, as in our previous papers and as described in Bellazzini et al. (2002). About  $10^5$  artificial stars were used to derive photometric errors and completeness in *B*, *V* and *I* exposures for the central chip. The resulting completeness fractions are shown in Table 3. For magnitudes brighter than 15, the completeness is 100%.

## 2.2 Calibration

No standard areas were observed during our observing night, thus we were forced to calibrate the cluster by using existing photometry. Unfortunately, neither Kaluzny & Mazur (1991, who have *UBV* images) nor Ann et al. (1999, *UBVI* images) cover the full FoV of LBC. The SDSS photometry cannot be used directly, because all bright targets (i.e., giants as well as stars at the Main Sequence Turn Off - MSTO) are saturated, so we used the SDSS to obtain calibration equations for each of the four chips, as done in Donati et al. (2015).

We transformed the SDSS *gri* magnitudes to the Johnson-Cousins *BVI* values<sup>3</sup>. The calibration equations are summarised in Table 4. They are in the form

$$M - m_i = zp + a \times C_i + b \times C_i^2$$

<sup>2</sup> We used the code CATAXCORR, developed by Paolo Montegriffo at the INAF - Osservatorio Astronomico di Bologna, see <http://www.bo.astro.it/~paolo/Main/CataPack.html>

<sup>3</sup> For the conversion we used the equations available at <http://www.sdss.org/dr4/algorithms/sdssUBVRITransform.html#Lupton2005>

**Table 4.** Calibration equations obtained for the four CCDs. For each equation 200 to 400 stars were used.

| CCD 1   |     |       |
|---|-----|-------|
| equation  | rms |       |
| $B - b = 4.505 - 0.494 \times (b - v) + 0.177 \times (b - v)^2$ | rms | 0.029 |
| $V - v = 4.253 - 0.076 \times (b - v)$                          | rms | 0.019 |
| $V - v = 4.249 - 0.055 \times (v - i)$                          | rms | 0.019 |
| $I - i = 4.175 - 0.015 \times (v - i)$                          | rms | 0.019 |
| CCD 2   |     |       |
| equation  | rms |       |
| $B - b = 4.484 - 0.542 \times (b - v) + 0.232 \times (b - v)^2$ | rms | 0.029 |
| $V - v = 4.224 - 0.062 \times (b - v)$                          | rms | 0.018 |
| $V - v = 4.225 - 0.050 \times (v - i)$                          | rms | 0.018 |
| $I - i = 4.133 - 0.011 \times (v - i)$                          | rms | 0.021 |
| CCD 3   |     |       |
| equation  | rms |       |
| $B - b = 4.489 - 0.554 \times (b - v) + 0.227 \times (b - v)^2$ | rms | 0.037 |
| $V - v = 4.226 - 0.065 \times (b - v)$                          | rms | 0.020 |
| $V - v = 4.209 - 0.036 \times (v - i)$                          | rms | 0.021 |
| $I - i = 4.095 - 0.014 \times (v - i)$                          | rms | 0.020 |
| CCD 4   |     |       |
| equation  | rms |       |
| $B - b = 4.423 - 0.341 \times (b - v) + 0.121 \times (b - v)^2$ | rms | 0.039 |
| $V - v = 4.221 - 0.068 \times (b - v)$                          | rms | 0.019 |
| $V - v = 4.209 - 0.039 \times (v - i)$                          | rms | 0.020 |
| $I - i = 4.102 - 0.009 \times (v - i)$                          | rms | 0.021 |

for *V* and *I*, and in the form

$$M - m_i = zp + a \times C_i + b \times C_i^2$$

for *B*, where we considered a quadratic dependence of the magnitude on the colour. *M* is the magnitude in the standard photometric system, *m<sub>i</sub>* the instrumental magnitude, *zp* the zero-point, *a* describes the linear dependence from the instrumental colour *C<sub>i</sub>*, and *b* describes the quadratic dependence on the instrumental colour *C<sub>i</sub>*. The comparisons with the original SDSS catalogue are shown in Fig. 2, where we show also the difference between the *V* magnitudes obtained with either the *B* - *V* or the *V* - *I* colours. We deem these comparisons satisfying; in particular, the difference between the two *V* magnitudes is negligible (less than 0.01 mag with a root mean square, hereafter rms, of the same order).

The final catalogue contains the identification, celestial coordinates, magnitudes and errors for 4791 stars. It will be made available through the BOCCE webpage ([www.bo.astro.it/?page\\_id=2632](http://www.bo.astro.it/?page_id=2632)), WEBDA<sup>4</sup>, and the Centre de Donnée de Strasbourg (CDS)<sup>5</sup>.

## 2.3 Comparison with literature

As mentioned in the Introduction, only two previous studies presented CCD photometry for this cluster (Kaluzny &

<sup>4</sup> <http://webda.physics.muni.cz>

<sup>5</sup> <http://cdsarc.u-strasbg.fr/viz-bin/qcat?J/MNRAS/>

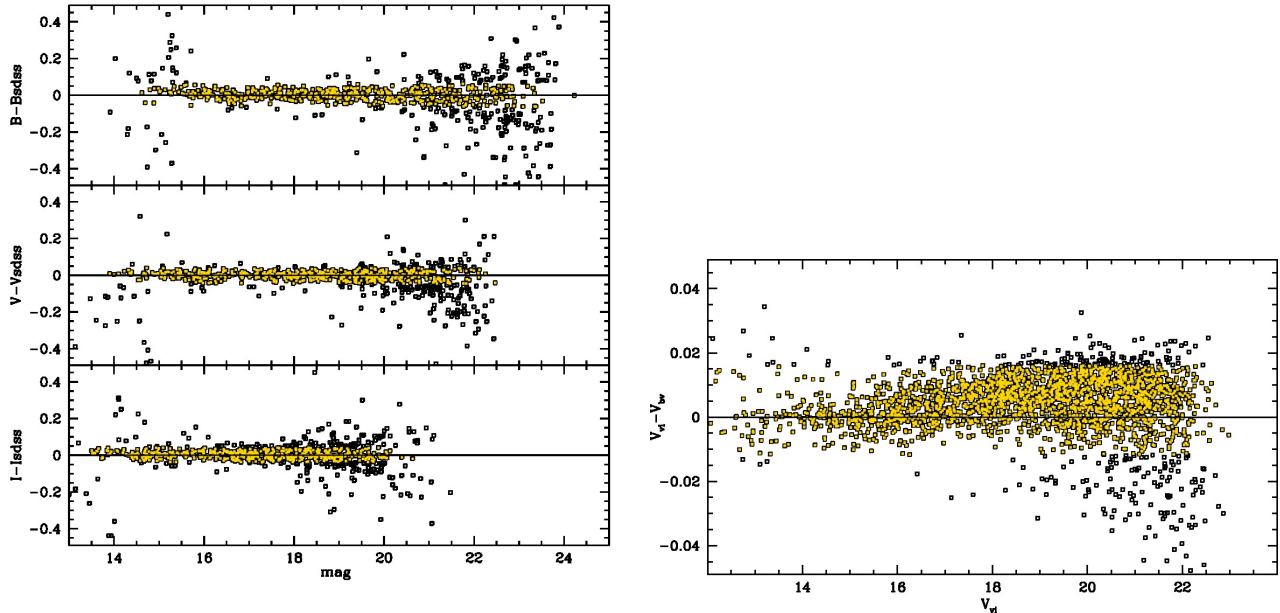


**Figure 2.** Left panel: Comparison of the calibrated  $B$ ,  $V$ , and  $I$  magnitudes with the SDSS photometry for CCD #2. The yellow-filled dots are the stars used to compute the mean difference within  $1\sigma$  from the average. The differences are consistent with 0, without trends with magnitude. The same conclusions apply to all the other CCDs of the instrument. Right panel: Comparison of the  $V$  obtained from  $b - v$  and the  $V$  obtained from  $v - i$ . A slight trend with magnitude is present; however, the average difference (again computed with the yellow filled dots within  $1\sigma$  from the average) is about 0.004 mag with an rms of 0.006 mag.

Mazur 1991; Ann et al. 1999). We downloaded their catalogues from the WEBDA and cross-identified stars with our photometry. In Fig. 3 we compare our photometry with theirs (upper panels for  $B, V$  and Kaluzny & Mazur 1991; lower panels for  $B, V, I$  and Ann et al. 1999); in both cases we reach deeper magnitudes and on a much larger field of view. As usual when doing these comparisons, there are small offsets between different photometries (always smaller than 0.05 mag, see numbers in the figure panels). In the case of the  $B$  magnitude, a colour term with both photometries is also present. This is absent in  $V$  when using Kaluzny and Mazur, whereas a small trend seems to be present in  $V$  or  $I$  with Ann et al.’s values<sup>6</sup>.

While the offsets are very small, the trend in  $B$  is annoying. So we checked that our calibration procedure through tertiary standard stars is not affected by significant photometric errors. We compared directly the  $B, V$  values of Kaluzny & Mazur (1991) and Ann et al. (1999) and we show the results in Fig. 4. A non-linear trend with magnitude is present in the  $B$  filter, in addition to an offset of almost 0.1 mag. In the case of  $V$ , the offset is smaller but a linear trend is evident. We are then unable to say which, if any, of the three calibrations is better; only an independent catalogue, obtained from observations in photometric conditions, may settle this issue. However, the total effect on the CMD is small, as apparent from Figure 3, and does not hamper the determination of the cluster parameters, producing at most a small difference in reddening and distance modulus esti-

mation, well within the errors of the determinations. Age is in fact mainly constrained by the difference in magnitude between the RC and TO stars, where offsets in  $V$  cancel out.

#### 2.4 Centre, diameter, CMD

Thanks to the precise and deep photometry of LBT and to its relatively large FoV, we re-determined the centre of the cluster following the approach described in Donati et al. (2012). Briefly, we selected the densest region on the images by looking for the smallest coordinates interval that contains 70% of all the stars. The centre is obtained as the average right ascension and declination when the selection is iterated twice. For a more robust estimate, several magnitude cuts have been considered iteratively and the corresponding results averaged. The rms on the centre coordinates is about  $5''$ . We found RA(J2000)=07:16:59.44, Dec(J2000)=+13:45:52.50, to be compared with the values cited in WEBDA (RA=07:16:59, Dec=+13:45:00 referred to J2000). From the density profile it was also possible to define the apparent diameter of the cluster. We estimated  $d = 9' \pm 1'$  using the radius at which the density profile flattens and reaches the background density value. For comparison, Soubiran et al. (2000) found that NGC 2355 has a central component reaching to about  $7'$ , while the radius at which the surface density drops to half the central value is  $1.5'$ .

Membership probability based on proper motions were published by Krone-Martins et al. (2010) for almost 400 stars in the field of NGC 2355, based on the PM2000 catalogue (Ducourant et al. 2006), complete to  $V \sim 15$  mag and with a limiting magnitude  $V \sim 16$  mag. Unfortunately,

<sup>6</sup> Note that the  $V - I$  calibration in Ann et al. (1999) appears problematic; they shifted the colours of the stars by 0.1 mag to match the same isochrone that fits the  $B - V$  colour (their Fig. 7).

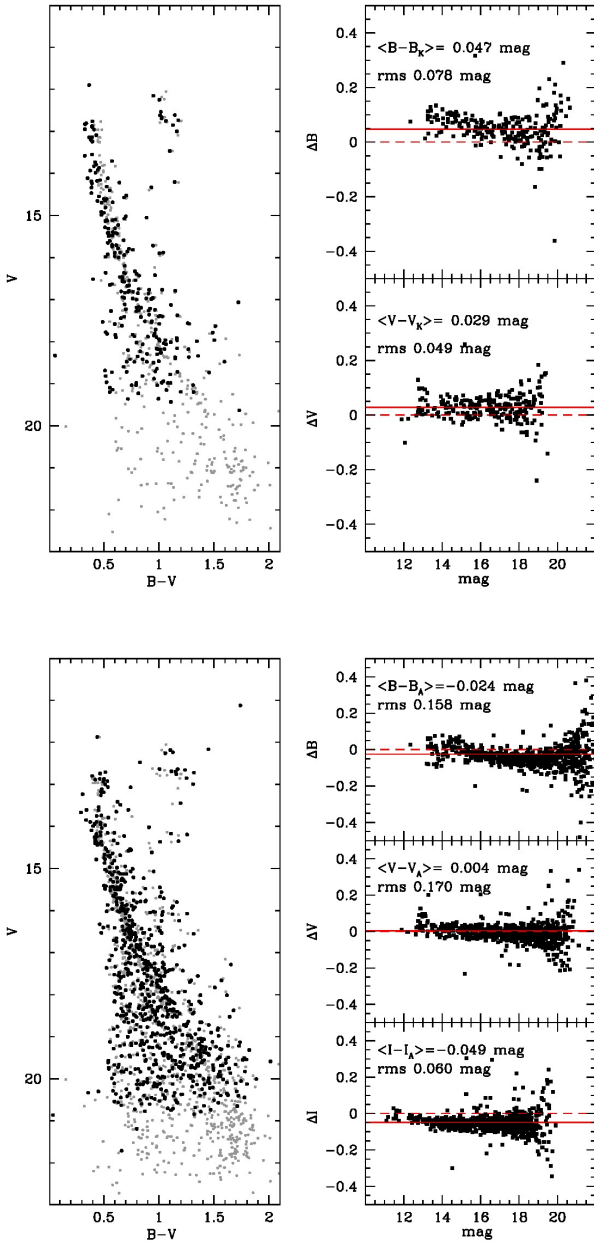


**Figure 3.** Comparison between our photometric catalogue and the literature ones. Upper panels: on the left the  $V, B - V$  CMD from Kaluzny & Mazur (1991) in black and our CMD on a area of the same size in gray; on the right the comparison of  $B$  and  $V$  magnitudes. The average differences and rms are indicated in the respective panels Lower panel: the same, but with the  $BVI$  photometry from Ann et al. (1999).

we cannot use these magnitudes to solve the problem of the differences among photometries, because they are not on the standard Johnson system (see Rapaport et al. 2001). However, this information is useful to better define the cluster evolutionary sequences. Krone-Martins et al. (2010) found 213 probable member stars; we cross-identified their catalogue with our photometry and use their membership determination and membership from RV (both analyses are in

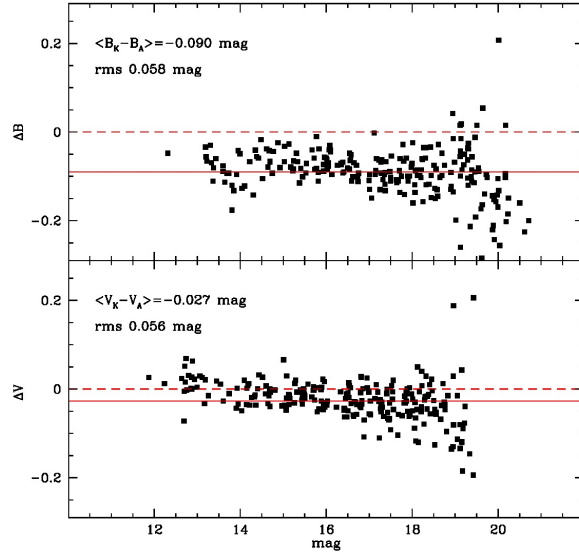


**Figure 4.** Photometric comparison between Kaluzny & Mazur (1991) and Ann et al. (1999) catalogues. Upper panel: there is an offset of about 0.1 mag in  $B$ , with a complex trend with magnitude. Lower panel: there is a smaller offset in the case of  $V$ , about 0.03 mag, but also an evident dependence on magnitude.

quite good agreement: 18 stars out of 23 in common between them are defined cluster members) to distinguish the cluster footprint (see Fig. 5) and to derive the cluster parameters (see Sec. 4).

NGC 2355 is not a very populous cluster, as shown by the CMD in Figure 5. However, the cluster MS is well distinguishable with respect to the field contamination. Field stars possess a complex pattern in the CMD, with at least three major components: a faint and blue MS, signature of a much more distant, older population, most likely the thick disc; an intermediate MS with stars defining an almost vertical sequence; and the vertical locus of M dwarfs, redder than the cluster MS, evident particularly in the  $V, B - V$  CMD. A study of the Galactic field population is beyond the scope of this paper, but it can be a side product of the BOCCE project, especially when large FoV are employed (see Cignoni et al. 2008, 2011).

Field interlopers, though mainly located below the cluster MS, complicate the interpretation of the upper MS, especially the identification of the red-hook (RH, the reddest point on the MS before the overall contraction evolutionary phase) and the giant phase which are poorly populated. Taking the membership into account, thanks to the radial velocity measures available in literature (see references in the Introduction) and the proper motion analysis (see Krone-Martins et al. 2010), it is possible to define the sequences of the cluster with more confidence. However, as apparent from Fig. 5, the identification of the RH is not straightforward. Therefore we decided to conservatively identify only the MS termination point (MSTP), as the brightest luminosity level reached by MS stars.

In Fig. 6 we show the CMDs of NGC 2355 for regions within different distances from the cluster centre ( $1'$ ,  $3'$ , and  $5'$ ) in comparison with an external area of  $5'$  radius. We

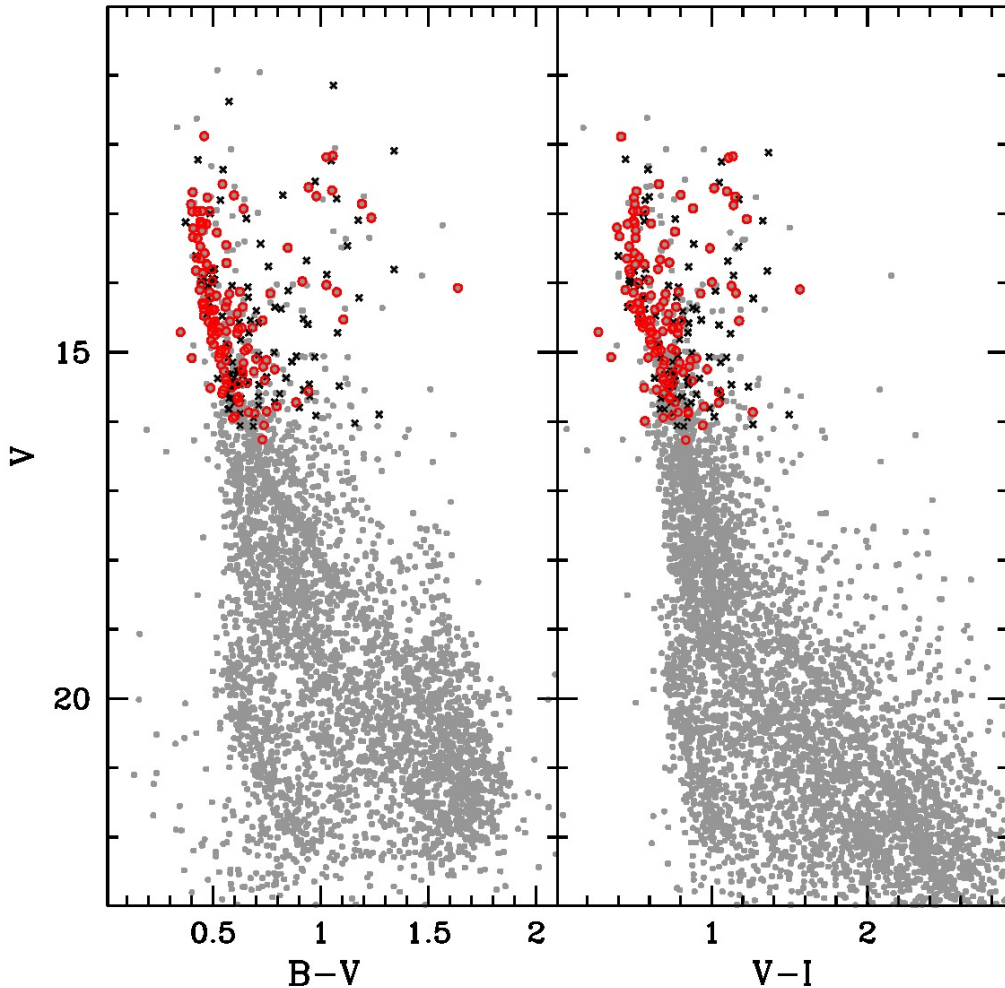


**Figure 5.** CMDs of NGC 2355 in  $V, B - V$  and  $V, V - I$  for the whole LBT FoV. In red we highlight probable members from Krone-Martins et al. 2010 (membership probability greater than 80%), whilst black crosses are probable non-members (membership probability lower than 50%).

identify a small gap at about  $V \sim 13.4$  mag on the MS, also found by both Kaluzny & Mazur (1991) and Ann et al. (1999); the occurrence of similar gaps is not uncommon, in open clusters (e.g., NGC 6134, Ahumada et al. 2013) and in principle can be related to the overall contraction phase, however the following analysis with synthetic CMDs (see Sec. 4) does not give a firm confirmation of this interpretation.

We used the radial plots and the membership probabilities to identify the evolutionary features of the cluster employed in the following analysis (see Sec. 4), and we identified:

- the RC and giants at  $V \sim 12.5$ ,  $(B - V) \sim 1$  mag;
- the MSTP at  $V \sim 13$  mag;
- and the MS extending down to  $V \sim 22$  mag.

### 3 SPECTROSCOPY

As already mentioned in the Introduction, several stars in NGC 2355 have been observed with high-resolution spectroscopy, but our study adds new important information. In fact, M08 only derived radial velocity (RV); S00 obtained rather low signal-to-noise ratio (S/N) spectra, useful for RV, atmospheric parameters, and metallicity, but not suitable for detailed chemical analysis. J11 have spectra covering only a limited wavelength range, so that only a few elements could be measured; finally, Jacobson & Friel (2013) observed only three stars. Thus our work doubles the number of stars for which abundances of elements forged by different nucleosynthetic chains can be determined in this cluster.

#### 3.1 Observation and reduction

We selected stars on the RC of NGC 2355 as possible targets, using the information from S00 and M08 to observe only members (see Table 5). We obtained high-resolution spectra

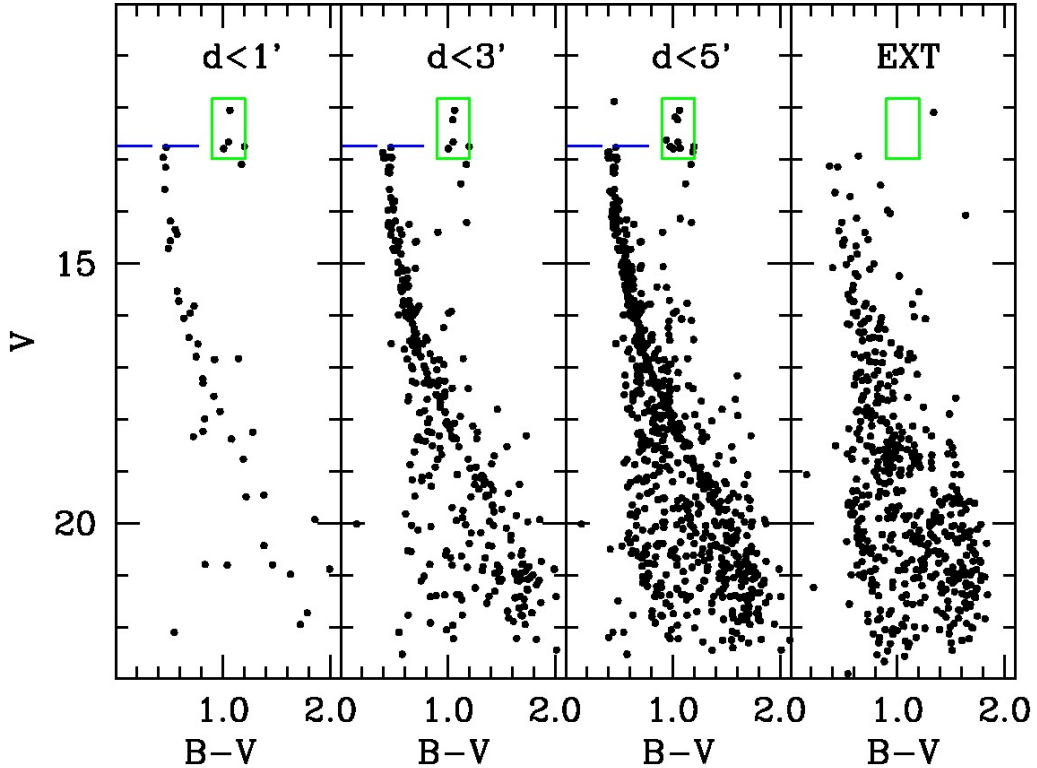


**Figure 6.** CMDs for regions within different distances from the cluster centre, compared with an external field of a circular area of  $5'$  radius. We highlight the MSTP and RC. For a better comparison, the RC box is shown also in the CMD of the external field.

of three RC stars using FIES (FIBre-fed Echelle Spectrograph) at the NOT (see Telting et al. 2014 for instrumentation details). FIES covers the range  $\lambda\lambda = 3700 - 7300 \text{ \AA}$  without gaps. We used the medium-resolution fibre bundle ( $R \equiv \lambda/\Delta\lambda = 46000$ ) and a  $2 \times 2$  binning to increase the S/N.

Information on the observed stars is provided in Table 6 and their position in the CMD is indicated in Fig. 7. Star #817 was observed in visitor mode in January 2014, while stars #536, 587 were subsequently observed in service mode (see Table 2). For the second star, no wavelength calibration frames were taken in the same night; we had to use the January lamps and this resulted in a lower precision in the zero point of the calibration. However, this is irrelevant to chemical analysis, but it results in a less precise RV measurement.

Star #817 was observed with three 1800s-long exposures while stars #536 and #587 had three 2100s-long exposures; they were reduced using the dedicated FIES software (FIESTOOL), which takes care of all standars steps, from bias subtraction to wavelength calibration. We cleaned the telluric contamination in a small region near the [O I] line and measured the RV on the final 1-d spectra using IRAF<sup>7</sup> routines and DAOSPEC (Stetson & Pancino 2008). The individual spectra were then shifted and co-added.

<sup>7</sup> IRAF is the Image Reduction and Analysis Facility, distributed by the National Optical Astronomy Observatory, which is operated by the Association of Universities for Research in Astronomy (AURA) under cooperative agreement with the National Science Foundation.

**Table 5.** Stars in common with S00, M08, J11 and their status.

| ID                              | WEBDA | ID(S00)     | S00 | M08 | J11 |
|---------------------------------|-------|-------------|-----|-----|-----|
| High-res spectra and photometry |       |             |     |     |     |
| 201728                          | 817   | km03        | yes | M   | ... |
| 201729                          | 536   | km04        | yes | M   | ... |
| 201735                          | 587   | km08        | yes | M   | ... |
| Only photometry                 |       |             |     |     |     |
| 201712                          | 335   | km19        | yes | ... | ... |
| 201715                          | 662   | km22        | yes | ... | ... |
| 201720                          | 441   | km21        | yes | ... | ... |
| 201726                          | 668   | GSC77500538 | yes | ... | M   |
| 201731                          | 276   | km02        | no  | ... | ... |
| 201732                          | 563   | km10        | yes | M   | M   |
| 201734                          | 832   | GSC77501264 | yes | ... | ... |
| 201736                          | 736   | km07        | no  | NM  | NM  |
| 201737                          | 734   | ...         | ... | ... | NM  |
| 201738                          | 592   | km09        | yes | M   | M   |
| 201739                          | 377   | km15        | yes | ... | M   |
| 201740                          | 599   | km20        | no  | SB  | ... |
| 201742                          | 734   | km12        | yes | ... | ... |
| 201744                          | 382   | km13        | yes | ... | ... |
| 201745                          | 296   | km14        | yes | ... | ... |
| 201752                          | 360   | ...         | ... | ... | NM  |
| 201754                          | 472   | km27        | yes | ... | ... |
| 301356                          | 144   | GSC77501198 | yes | ... | M   |

KM is the identifier in Kaluzny & Mazur (1991)

M09, J11 use the WEBDA identifier.

yes,M : member stars ; NM : not a member ; SB: binary

**Table 6.** Data for the three stars with high-resolution spectra.

| ID     | WEBDA | other | RA<br>(J2000) | Dec<br>(J2000) | B      | V      | S/N | RV<br>km/s      | T <sub>eff</sub> | logg | <i>v<sub>t</sub></i> | [Fe/H] |
|--------|-------|-------|---------------|----------------|--------|--------|-----|-----------------|------------------|------|----------------------|--------|
| 201728 | 817   | KM03  | 109.2414551   | +13.7734194    | 13.116 | 12.050 | 80  | 35.57           | 5080             | 2.64 | 1.16                 | -0.01  |
| 201729 | 536   | KM04  | 109.2476883   | +13.7881250    | 13.283 | 12.234 | 90  | 39 <sup>a</sup> | 4998             | 2.41 | 1.19                 | -0.04  |
| 201735 | 587   | KM08  | 109.2376022   | +13.7740917    | 13.714 | 12.662 | 110 | 35.44           | 5110             | 2.88 | 1.13                 | -0.15  |

Notes - other=Kaluzny & Mazur (1991).

<sup>a</sup> The RV for star 536 is uncertain (see text).

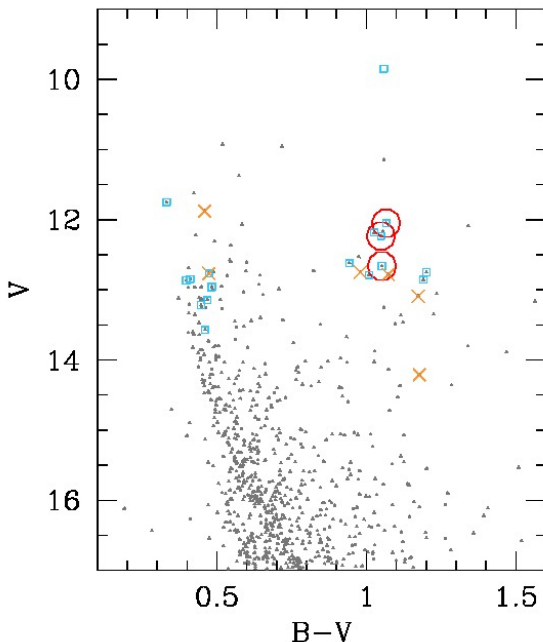


**Figure 7.** CMD of NGC 2355 with the three stars observed with NOT@FIES indicated by large red circles. Light blue squares indicate member stars and orange crosses non members (from Soubiran et al. 2000; Mermilliod et al. 2008; Jacobson et al. 2011b) in common with our photometry.

### 3.2 Atmospheric parameters and iron abundances

These three spectra were analysed as in other BOCCE clusters and we give here only a short description of the procedure; for more details see Bragaglia et al. (2001, 2006a); Carretta et al. (2004, 2005). Equivalent widths (EWs) were measured employing an updated version of the ROSA spectrum analysis package (Gratton 1988). We restricted to the 5500-7000 Å spectral range for Fe lines to minimize problems of line crowding and difficult continuum tracing blueward of this region and of contamination by telluric lines redward. We employed the entire spectrum for other elements. Sources of oscillator strengths and atomic parameters are the same as in Gratton et al. (2003).

We used as initial guesses for effective temperature ( $T_{\text{eff}}$ ) and gravity ( $\log g$ ) the values based on photometric data, the Alonso, Arribas, & Martínez-Roger (1999) relations, distance, and reddening. We then derived the final values for  $T_{\text{eff}}$  and  $\log g$  from the spectra using the excitation and ionisation equilibria for iron, respectively. The microturbulent

velocity ( $v_t$ ) was derived assuming the relation between  $\log g$  and  $v_t$  given in Carretta et al. (2004), i.e.,  $v_t = 1.5 \times \log g$ . These parameters, along with iron abundances, are reported in Table 6.

The iron abundances derived from EWs were checked using synthetic spectra of about 30 selected iron lines (see Carretta et al. 2004, for a description of these lines). The average differences between iron abundance based on EW and on synthesis is 0.1 dex, without systematic trends. We are then confident to have achieved the accuracy in continuum tracing and EW measurements possible with these spectra. The average values we found for the three stars are  $[\text{Fe/H}]_{\text{I}} = -0.064 \pm 0.044$  (rms=0.076) dex, and  $[\text{Fe/H}]_{\text{II}} = -0.066 \pm 0.043$  (rms=0.075) dex. The very good agreement between the values for two ionisation states (found also for Ti and Cr, see later) is a further confirmation of the surface gravities.

We derived errors in EWs, temperature, gravity, model metallicity, and microturbulent velocity taking into account that they are not independent. Errors were estimated as in Carretta et al. (2004) where a detailed description is given. They comprise a) a random part different from star-to-star (due, for example, to the different S/N ratios) that represents the internal error; and b) a systematic part (due, for example, to uncertainties in the adopted oscillator strengths, blends not considered, etc.). Random errors have been found to be of 25 K in  $T_{\text{eff}}$ , 0.07 dex in  $\log g$ , and  $0.17 \text{ km s}^{-1}$  in  $v_t$ . In Table 7 we present the sensitivity of the derived abundance ratios to the variations in atmospheric parameters and to errors in EWs, obtained by repeating our abundance analysis by changing only one parameter at the time. The amount of the changes is shown in the first line of the header, the random error used to determine the resulting abundance changes is given in the second line, and the corresponding variations are given for all elements separately for each parameter and as a total (internal) variation.

### 3.3 Other elements

We derived abundances for O, the light elements Na and Al, the  $\alpha$ -process elements Mg, Si, Ca, Ti (from Ti I and II lines), the Fe-group elements Sc, Cr (from neutral and singly-ionised features), Mn, Ni, Cu, Zn, and for the neutron-capture elements Y, Zr, Ba, La, Ce, Pr, Nd, Eu. The abundance ratios for the three stars are given in Table 8, together with the number of lines used, the abundance by number, and the rms.

As done in previous works of the series, most of the abundances were derived using EWs; we took hyperfine structure into consideration for Sc and Mn and the abun-

**Table 7.** Sensitivities of abundance ratios to variations in the atmospheric parameters and to errors in the equivalent widths (or fit, for spectreum synthesis), and errors in abundances for stars of NGC 2355.

| Element   | Average<br>n. lines | $T_{\text{eff}}$<br>(K) | $\log g$<br>(dex) | [A/H]<br>(dex) | $v_t$<br>$\text{km s}^{-1}$ | EWs<br>(dex) | Total<br>Internal | Note |
|-----------|---------------------|-------------------------|-------------------|----------------|-----------------------------|--------------|-------------------|------|
| Variation |                     | 50                      | 0.20              | 0.10           | 0.10                        |              |                   |      |
| Internal  |                     | 25                      | 0.07              | 0.07           | 0.17                        | 0.06         |                   |      |
| [Fe/H]I   | 108                 | +0.038                  | -0.001            | +0.004         | -0.040                      | 0.005        | 0.071             | EW   |
| [Fe/H]II  | 14                  | -0.032                  | +0.095            | +0.031         | -0.033                      | 0.015        | 0.073             | EW   |
| [O/Fe]I   | 2                   | -0.031                  | +0.089            | +0.036         | +0.039                      | 0.040        | 0.089             | EW   |
| [Na/Fe]I  | 4                   | -0.004                  | -0.022            | +0.002         | +0.014                      | 0.029        | 0.038             | EW   |
| [Mg/Fe]I  | 3                   | -0.013                  | -0.008            | -0.005         | +0.022                      | 0.033        | 0.050             | EW   |
| [Al/Fe]I  | 2                   | -0.008                  | -0.007            | -0.006         | +0.029                      | 0.040        | 0.064             | EW   |
| [Si/Fe]I  | 13                  | -0.035                  | +0.050            | +0.012         | +0.055                      | 0.016        | 0.099             | EW   |
| [Ca/Fe]I  | 14                  | +0.010                  | -0.028            | -0.007         | -0.010                      | 0.015        | 0.026             | EW   |
| [Sc/Fe]II | 6                   | +0.026                  | -0.009            | +0.000         | -0.011                      | 0.023        | 0.033             | EW   |
| [Ti/Fe]I  | 9                   | +0.025                  | -0.004            | -0.007         | +0.013                      | 0.019        | 0.032             | EW   |
| [Ti/Fe]II | 1                   | +0.022                  | -0.005            | +0.003         | +0.027                      | 0.057        | 0.074             | EW   |
| [Cr/Fe]I  | 10                  | +0.005                  | -0.006            | -0.004         | +0.018                      | 0.018        | 0.036             | EW   |
| [Cr/Fe]II | 2                   | +0.003                  | -0.008            | -0.006         | +0.020                      | 0.040        | 0.053             | EW   |
| [Mn/Fe]I  | 4                   | +0.016                  | -0.036            | +0.002         | -0.029                      | 0.029        | 0.059             | EW   |
| [Cu/Fe]I  | 1                   | +0.050                  | +0.040            | +0.040         | +0.030                      | 0.050        | 0.095             | SS   |
| [Ni/Fe]I  | 35                  | -0.008                  | +0.020            | +0.006         | +0.008                      | 0.010        | 0.019             | EW   |
| [Zn/Fe]I  | 1                   | -0.049                  | +0.049            | +0.021         | -0.005                      | 0.057        | 0.067             | EW   |
| [Y/Fe]II  | 3                   | +0.050                  | +0.030            | +0.000         | +0.090                      | 0.035        | 0.111             | SS   |
| [Zr/Fe]I  | 3                   | +0.044                  | -0.002            | -0.002         | +0.039                      | 0.033        | 0.077             | EW   |
| [Zr/Fe]II | 1                   | +0.029                  | -0.007            | +0.003         | +0.017                      | 0.057        | 0.066             | EW   |
| [Ba/Fe]II | 4                   | +0.030                  | +0.050            | +0.000         | +0.080                      | 0.006        | 0.099             | SS   |
| [La/Fe]II | 3                   | +0.040                  | +0.050            | +0.020         | +0.050                      | 0.021        | 0.085             | SS   |
| [Ce/Fe]II | 1                   | +0.038                  | -0.008            | +0.006         | +0.014                      | 0.057        | 0.065             | EW   |
| [Pr/Fe]II | 3                   | +0.039                  | -0.009            | +0.007         | +0.026                      | 0.033        | 0.059             | EW   |
| [Nd/Fe]II | 2                   | +0.030                  | +0.040            | +0.020         | +0.050                      | 0.028        | 0.079             | SS   |
| [Sm/Fe]II | 2                   | +0.045                  | -0.007            | +0.010         | +0.011                      | 0.040        | 0.050             | EW   |
| [Eu/Fe]II | 2                   | +0.050                  | +0.050            | +0.000         | +0.060                      | 0.070        | 0.116             | SS   |

dance of Na was corrected for departures from local thermodynamic equilibrium (LTE) according to Gratton et al. (1999). For O, we checked the abundance also with spectrum synthesis.

Abundance analyses for Cu and the neutron-capture elements Y, Ba, La, Nd, and Eu have been carried out via spectral synthesis calculations using MOOG (Sneden 1973, 2014 version) and the Kurucz (1993) grid of model atmospheres, with solar-scaled composition and convective overshooting. This is different from what we did in past papers so a few details on the features used are given below.

Copper abundances were determined from the 5782 Å line, taking into account the hyperfine structure (from Steffen 1985) and adopting isotopic ratios of 69% and 31% for  $^{63}\text{Cu}$  and  $^{65}\text{Cu}$ , respectively.

We employed a single-line treatment for Y II lines at 4884 Å, 4900 Å, and 5729 Å. For the first two spectral features we adopted the same line lists as in D’Orazi et al. (2013), whereas atomic parameters ( $\chi=1.84$  eV,  $\log g f=-1.12$ ) for the line at 5728 Å come from Thygesen et al. (2014). McWilliam et al. (2013) published hyperfine structure splitting for the last spectral line (with a total  $\log g f$  of -0.99). However, we checked that the difference in the resulting abundance with respect to a single-line treatment is relatively small (0.05 dex), which is well within our observational uncertainties. This is not surprising, because, although the main Y isotope ( $^{89}\text{Y}$ ) has an odd mass num-

ber, the level splitting is negligible, given the small spin and magnetic momentum of the yttrium nucleus. Thus, for sake of consistency with the other lines under consideration in the present study we did not include hyperfine splittings. The standard deviation (see Table 9) of the average Y abundances ensures us that our assumption is quite reasonable.

Ba abundances were inferred by analysing single-ionised features at 5853 Å, 6141 Å and 6496 Å, adopting hyperfine and isotopic splitting following Mc William (1998) and assuming solar mixtures for the Ba isotopes, namely 81% for ( $^{134}\text{Ba} + ^{136}\text{Ba} + ^{138}\text{Ba}$ ) and 19% for ( $^{135}\text{Ba} + ^{137}\text{Ba}$ ), as in our previous works (see e.g., D’Orazi et al. 2012).

The  $\log g f$  for all the components for La II lines at 4748 Å, 4804 Å, and 6390 Å and Eu II at 6645 Å were retrieved from Lawler, Bonvallet & Sneden (2001) and Lawler et al. (2001), respectively. In the latter case isotopic ratios of 48% and 52% for  $^{151}\text{Eu}$  and  $^{153}\text{Eu}$ , respectively, were chosen.

Finally, Nd abundances come from Nd II spectral features at 5740 Å and 5811 Å, with atomic parameters provided by Den Hartog et al. (2003).

In Table 9 we give the average abundance ratios for three elements measured in the three stars of NGC 2355, together with the error and rms. We also give the solar reference values adopted in the analysis.

**Table 8.** Abundances for the three stars; we indicate when spectrum synthesis (SS) or equivalent widths (EW) were used.

| element               | 201729 |       |        |       | 201728 |       |        |       | 201735 |       |        |       | Note |
|-----------------------|--------|-------|--------|-------|--------|-------|--------|-------|--------|-------|--------|-------|------|
|                       | nr     | logn  | [X/Fe] | rms   | nr     | logn  | [X/Fe] | rms   | nr     | logn  | [X/Fe] | rms   |      |
| [Fe/H] <sub>I</sub>   | 108    | 7.500 | -0.040 | 0.102 | 107    | 7.536 | -0.004 | 0.094 | 109    | 7.391 | -0.149 | 0.070 | EW   |
| [Fe/H] <sub>II</sub>  | 14     | 7.443 | -0.047 | 0.080 | 14     | 7.488 | -0.002 | 0.094 | 13     | 7.341 | -0.149 | 0.067 | EW   |
| [O/Fe]                | 2      | 8.524 | -0.226 | 0.075 | 2      | 8.380 | -0.406 | 0.010 | 1      | 8.558 | -0.083 |       | EW   |
| [Na/Fe]               | 4      | 6.353 | 0.183  | 0.042 | 4      | 6.383 | 0.177  | 0.074 | 4      | 6.200 | 0.139  | 0.138 | EW   |
| [Mg/Fe]               | 3      | 7.456 | 0.066  | 0.082 | 3      | 7.425 | -0.001 | 0.026 | 3      | 7.410 | 0.129  | 0.073 | EW   |
| [Al/Fe]               | 2      | 6.114 | -0.076 | 0.091 | 2      | 6.249 | 0.023  | 0.093 | 2      | 6.123 | 0.042  | 0.117 | EW   |
| [Si/Fe]               | 14     | 7.549 | 0.059  | 0.097 | 14     | 7.537 | 0.011  | 0.119 | 12     | 7.415 | 0.034  | 0.073 | EW   |
| [Ca/Fe]               | 14     | 6.386 | 0.156  | 0.091 | 16     | 6.372 | 0.106  | 0.114 | 13     | 6.216 | 0.095  | 0.123 | EW   |
| [Ti/Fe] <sub>I</sub>  | 8      | 4.850 | -0.110 | 0.083 | 9      | 4.953 | -0.043 | 0.061 | 9      | 4.815 | -0.036 | 0.061 | EW   |
| [Ti/Fe] <sub>II</sub> | 1      | 4.904 | -0.119 |       | 1      | 4.947 | -0.121 |       | 2      | 4.825 | -0.096 | 0.030 | EW   |
| [Sc/Fe] <sub>II</sub> | 5      | 3.069 | -0.014 | 0.111 | 7      | 3.071 | -0.057 | 0.069 | 5      | 2.949 | -0.032 | 0.149 | EW   |
| [Cr/Fe] <sub>I</sub>  | 9      | 5.571 | -0.059 | 0.129 | 10     | 5.620 | -0.046 | 0.121 | 10     | 5.484 | -0.037 | 0.124 | EW   |
| [Cr/Fe] <sub>II</sub> | 1      | 5.576 | -0.087 |       | 1      | 5.663 | -0.045 |       | 3      | 5.534 | -0.027 | 0.011 | EW   |
| [Mn/Fe]               | 3      | 5.444 | 0.144  | 0.057 | 3      | 5.391 | 0.055  | 0.039 | 6      | 5.224 | 0.033  | 0.141 | EW   |
| [Cu/Fe]               | 1      |       | -0.25  |       | 1      |       | -0.30  |       | 1      |       | -0.20  |       | SS   |
| [Ni/Fe]               | 34     | 6.125 | -0.115 | 0.068 | 34     | 6.183 | -0.093 | 0.089 | 36     | 6.080 | -0.051 | 0.070 | EW   |
| [Zn/Fe]               | 1      | 4.491 | -0.059 |       | 2      | 4.495 | -0.091 | 0.029 | 1      | 4.487 | 0.046  |       | EW   |
| [Y/Fe] <sub>II</sub>  | 2      |       | -0.05  | 0.05  | 2      |       | -0.18  | 0.13  | 2      |       | -0.10  | 0.10  | SS   |
| [Zr/Fe] <sub>I</sub>  | 3      | 2.363 | -0.190 | 0.034 | 3      | 2.390 | -0.208 | 0.037 | 3      | 2.319 | -0.132 | 0.022 | EW   |
| [Zr/Fe] <sub>II</sub> | 1      | 2.363 | -0.190 |       | 1      | 2.378 | -0.220 |       | 1      | 2.329 | -0.122 |       | EW   |
| [Ba/Fe] <sub>II</sub> | 3      |       | 0.20   | 0.01  | 3      |       | -0.03  | 0.03  | 3      |       | -0.03  | 0.04  | SS   |
| [La/Fe] <sub>II</sub> | 2      |       | 0.12   | 0.03  | 2      |       | 0.04   | 0.04  | 2      |       | 0.20   | 0.01  | SS   |
| [Ce/Fe] <sub>II</sub> | 1      | 1.701 | 0.118  |       | 1      | 1.737 | 0.109  |       | 1      | 1.731 | 0.250  |       | EW   |
| [Pr/Fe] <sub>II</sub> | 3      | 0.561 | -0.102 | 0.088 | 3      | 0.536 | -0.172 | 0.130 | 4      | 0.739 | 0.178  | 0.138 | EW   |
| [Nd/Fe] <sub>II</sub> | 2      |       | 0.03   | 0.04  | 2      |       | -0.03  | 0.04  | 2      |       | 0.16   | 0.05  | SS   |
| [Eu/Fe] <sub>II</sub> | 1      |       | -0.40  |       | 1      |       | -0.40  |       | 1      |       | -0.25  |       | SS   |

### 3.4 Comparison with previous spectroscopy

Mermilliod et al. (2008) used CORAVEL at the OHP (Observatoire Haute Provence) to obtain repeated RV measures of 12 stars in NGC 2355. Four were found to be not members and one of the eight members is a binary. The average RV of the seven single members is  $35.02 \pm 0.16$  (rms=0.42)  $\text{km s}^{-1}$ . Table 11 shows the comparison of our and their RVs; they are in very good agreement.

To derive the cluster's properties, Soubiran et al. (2000) combined spectra obtained with ELODIE on the 1.93m telescope at the OHP with the Kaluzny & Mazur (1991) photometry, 2MASS data, and proper motions. They obtained spectra of 24 stars, both evolved and at the MSTO; 17 turned out to be member on the basis of their RV. The eight stars near the MSTO have high rotational velocities; the average RV defined by the nine giants is  $35.13$  (rms=0.39)  $\text{km s}^{-1}$ , also in agreement with our values. Soubiran et al. (2000) used TGMET, a software which finds the best matching template in a library, to derive atmospheric parameters and absolute magnitude of the stars (see their Fig. 7 and Table 2). We observed three stars in common and Table 11 shows that there is a satisfactory agreement between our studies.

Jacobson et al. (2011b) observed NGC 2355 with the multiobject spectrograph Hydra at the 3.5m WYIN telescope on Kitt Peak; the resolution was about 18000 and the wavelength coverage about 300 Å, centred at 6280 Å. They obtained spectra for a dozen stars, half of which were found member (see their paper for details and for comparison with previous results, usually -but not-always- in good agreement). Abundance analysis was based on EWs and syn-

thesis, using MOOG (Sneden 1973). Finally, Jacobson & Friel (2013) observed three of these stars with the echelle spectrograph on the KPNO 4m telescope. None of our three stars is in common with these two studies. However, the average temperatures and gravities are 4975, 2.97 and 5200, 2.95 for the four RC stars in Jacobson et al. (2011b) and the two RC stars in Jacobson & Friel (2013), respectively, compared to our average values of 5062, 2.64.

We present in Table 10 a comparison between our average abundance ratios and those in Jacobson et al. (2011b) and Jacobson & Friel (2013) for the species in common. The metallicity agrees very well, whereas we find differences of the order of 0.1 dex for the light,  $\alpha$ , and iron-peak elements (given only in Jacobson et al. 2011b). This is a common occurrence when comparing inhomogeneous analyses and can be due to many factors such as different solar reference values (as in the cases of Na and Ca, where this would explain fully the offsets), different choice of lines,  $\log gf$ , temperatures, etc. Given the small offsets, we do not explore further these cases.

Very large discrepancies are found instead for the three neutron-capture elements Zr, Ba, and Eu; conversely, there is a very good agreement for the lanthanum abundances. This deserve investigation. Unfortunately, we have no stars in common, thus a direct comparison is hampered.

For Zr, we found a ratio of  $[\text{Zr/Fe}] = -0.18$  to be compared to  $[\text{Zr/Fe}] = +0.49$  by Jacobson & Friel (2013), implying a difference of 0.67 dex (more than a factor of four).

We can only partially explain such a large disagreement in terms of the adopted atomic parameters. Those authors discussed that their oscillator strengths results in a solar Zr

**Table 9.** Cluster averages and solar reference abundances

| element               | mean   | $\pm$ | rms   | Sun  |
|-----------------------|--------|-------|-------|------|
| [Fe/H] <sub>I</sub>   | -0.064 | 0.044 | 0.076 | 7.54 |
| [Fe/H] <sub>II</sub>  | -0.066 | 0.043 | 0.075 | 7.49 |
| [O/Fe]                | -0.238 | 0.094 | 0.162 | 8.79 |
| [Na/Fe]               | 0.166  | 0.014 | 0.024 | 6.21 |
| [Mg/Fe]               | 0.065  | 0.038 | 0.065 | 7.43 |
| [Al/Fe]               | -0.004 | 0.036 | 0.063 | 6.23 |
| [Si/Fe]               | 0.035  | 0.014 | 0.024 | 7.53 |
| [Ca/Fe]               | 0.119  | 0.019 | 0.033 | 6.27 |
| [Ti/Fe] <sub>I</sub>  | -0.063 | 0.024 | 0.041 | 5.00 |
| [Ti/Fe] <sub>II</sub> | -0.112 | 0.008 | 0.014 | 5.07 |
| [Sc/Fe] <sub>II</sub> | -0.034 | 0.013 | 0.022 | 3.13 |
| [Cr/Fe] <sub>I</sub>  | -0.047 | 0.006 | 0.011 | 5.67 |
| [Cr/Fe] <sub>II</sub> | -0.053 | 0.018 | 0.031 | 5.71 |
| [Mn/Fe]               | 0.077  | 0.034 | 0.059 | 5.34 |
| [Cu/Fe]               | -0.250 | 0.029 | 0.050 | 4.19 |
| [Ni/Fe]               | -0.086 | 0.019 | 0.033 | 6.28 |
| [Zn/Fe]               | -0.035 | 0.042 | 0.072 | 4.59 |
| [Y/Fe] <sub>II</sub>  | -0.110 | 0.038 | 0.066 | 2.21 |
| [Zr/Fe] <sub>I</sub>  | -0.177 | 0.023 | 0.040 | 2.60 |
| [Zr/Fe] <sub>II</sub> | -0.177 | 0.029 | 0.050 | 2.60 |
| [Ba/Fe] <sub>II</sub> | 0.047  | 0.077 | 0.133 | 2.18 |
| [La/Fe] <sub>II</sub> | 0.120  | 0.046 | 0.080 | 1.10 |
| [Ce/Fe] <sub>II</sub> | 0.159  | 0.046 | 0.079 | 1.63 |
| [Pr/Fe] <sub>II</sub> | -0.032 | 0.107 | 0.185 | 0.71 |
| [Nd/Fe] <sub>II</sub> | 0.053  | 0.056 | 0.097 | 1.45 |
| [Eu/Fe] <sub>II</sub> | -0.350 | 0.050 | 0.087 | 0.52 |

**Table 10.** Comparison of average abundances.

|         | here  | F11   | JF    | Sun lit. |
|---------|-------|-------|-------|----------|
| [Fe/H]  | -0.06 | -0.08 | -0.04 | 7.52     |
| [Na/Fe] | +0.17 | 0.05  | ...   | 6.33     |
| [Mg/Fe] | +0.07 | 0.21  | ...   | 7.58     |
| [Si/Fe] | +0.04 | 0.19  | ...   | 7.55     |
| [Ca/Fe] | +0.12 | 0.05  | ...   | 6.36     |
| [Ti/Fe] | -0.06 | -0.04 | ...   | 4.99     |
| [Ni/Fe] | -0.09 | 0.02  | ...   | 6.23     |
| [Zr/Fe] | -0.18 | 0.24  | 0.49  | 2.95     |
| [Ba/Fe] | +0.05 | ...   | 0.58  | 2.31     |
| [La/Fe] | +0.12 | ...   | 0.18  | 1.21     |
| [Eu/Fe] | -0.35 | ...   | -0.02 | 0.51     |

abundance larger than all literature estimates by  $\sim 0.3\text{--}0.4$  dex (see that paper for details). However, for Zr I lines in common with that study the average differences in  $\log g$  values are approximately 0.15 dex, so that they cannot account for the discrepancy. It is noteworthy that our Zr abundances from neutral and single-ionised lines do agree very well, sug-

**Table 11.** Literature values for the three stars.

| ID     | RV<br>(M08) | RV<br>(S00) | T <sub>eff</sub><br>(S00) | logg<br>(S00) | [Fe/H]<br>(S00) |
|--------|-------------|-------------|---------------------------|---------------|-----------------|
| 201728 | 34.07       | 34.79       | 4987                      | 2.72          | -0.14           |
| 201729 | 34.51       | 34.89       | 4961                      | 2.67          | -0.15           |
| 201735 | 34.58       | 35.73       | 5122                      | 2.73          | -0.23           |

M08=Mermilliod et al. (2008), S00=Soubiran et al. (2000)

gesting that the different ionisation stage of the lines under scrutiny is not responsible for the mismatch. On the other hand, we note also that in Jacobson & Friel (2013) there is a large scatter from different Zr I lines for two of the three stars, with values ranging from +0.19 to +0.60, and from +0.59 to +0.92, respectively. This seem to suggest that the [Zr/Fe] ratios could be quite uncertain and must be taken with caution.

The *r*-process element Eu presents a difference (in the sense ours minus Jacobson & Friel 2013) of  $-0.33$  dex, which is beyond measurement errors. While from our data the Eu content is very homogeneous within the cluster, Jacobson & Friel (2013) detected significant internal variations, finding a difference between star #144 and stars #398, 668 of a factor of two and four, respectively, in their [Eu/Fe] ratios. These differences seem due to one of the two lines they used; had they relied only on the same line we also are using (6645 Å), results would have been much more homogenous and more similar to our values (however, this line has been measured only in two of the three stars). Since open clusters are not known to host any intrinsic internal variations in terms of chemical composition, we are tempted to conclude that our analysis and the use of the best line is more robust.

Finally, given its peculiar pattern observed in open cluster stars, Ba deserves a more detailed discussion. First identified by D’Orazi et al. (2009), and subsequently confirmed by several different studies (e.g., Jacobson & Friel 2013, see discussion in Section 6), there is a trend of decreasing Ba abundances as a function of the open cluster’s age, with younger clusters exhibiting [Ba/Fe] ratios up to  $\sim 0.6$  dex (such as e.g., the case of IC 2602 and IC 2391 by D’Orazi et al. 2009), whereas solar ratios are measured for clusters a few Gyr old. Considering the age of NGC 2355, and values reported in the literature for almost coeval clusters, we should expect enhancements in the Ba content at levels of approximately 0.25–0.40 dex, which is not evident from the present analysis. In fact, our average mean abundance results in a solar [Ba/Fe] ratio of  $0.05 \pm 0.08$  dex (0.53 dex lower than Jacobson’s study). The different techniques and approaches could in principle explain this large discrepancy; for instance, equivalent width analysis has been carried out by D’Orazi et al. 2009 and Jacobson & Friel 2013, whereas here we performed spectral syntheses. Critical in this respect is also the microturbulence value, because Ba II lines sit on the saturated part of the curve of growth and they are quite insensitive to the abundance. Given the quite limited sample, we cannot certainly state that this cluster presents an anomalously low Ba content (considering its age) or, conversely, measurement errors cause this trend. Homogeneous analysis of all the data, or of a similarly large sample of clusters, should be attempted, to clarify this issue.

#### 4 SYNTHETIC CMDs

To complete our analysis of NGC 2355, the age, distance modulus, reddening (total and differential), and binary fraction of the cluster are estimated using the synthetic CMD technique (see Tosi et al. 1991) as done in all the papers of the BOCCE project (see e.g., Cignoni et al. 2011; Donati et al. 2012, 2014a and references therein). Homogeneous sets

of three types of stellar evolution models<sup>8</sup> are used to build a library of synthetic CMDs. Cluster parameters are determined by means of the comparison of the synthetic CMDs with the observed ones. The best-fitting solution is chosen as the one that can best reproduce age-sensitive indicators: the MSTP, the RC luminosity, the MS inclination and colour, and the RC colour. In order to make a meaningful comparison, the synthetic CMDs are made taking into account the photometric error, the completeness level of the photometry and the stellar density contrast of the OC population with respect to the population of an external field. The synthetic CMDs are combined with stars picked from an equal area of the external field to take the contamination into account.

Multi-colour photometry has generally proven to be fundamental to obtain the best parameters estimation. Hence, the best-fitting solutions are the ones that can reproduce at the same time all the observed CMDs (in our case,  $V, B - V$  and  $V, V - I$ ) for appropriate distance modulus, reddening, metallicity, and age. For NGC 2355 we fixed the metallicity of the models to the spectroscopic one (i.e. we adopted the evolutionary tracks with solar value:  $Z = 0.02$ ), which helped us restricting the possible range of parameters. With this metallicity we obtained a good fit of both  $V, B - V$  and  $V, V - I$  observational CMDs after adopting the standard extinction law ( $E(V - I) = 1.25 \times E(B - V)$ ,  $R_V = 3.1$ , see Dean, Warren, & Cousins 1978), circumstance that further confirms the spectroscopic metallicity and indirectly supports the accuracy of our calibration.

#### 4.1 Cluster parameters

The best solution for each set of tracks is the one whose synthetic CMD fits most of the visible MS shape, the RC and MSTP levels, the binary sequence, and, if present, the broadening of the MS due to differential reddening. In general we found RC colour slightly redder in the synthetic CMDs than in the observed one, especially in the  $V, B - V$  case. However, this evolutionary stage strongly depends on fundamental parameters (e.g. metallicity, age, helium content), and on physical inputs (e.g. efficiency of core overshooting, mass loss) to which colour is very sensitive. We also found an overall good agreement for the MS in the  $V, V - I$  CMD and a worse fit in the case of the  $V, B - V$  one, where the correct inclination of the sequence is not well reproduced. This is a rather common occurrence and probably the main driver of this mismatch is the uncertainty in the adopted temperature-colour transformations and in the model atmospheres (as discussed in Bragaglia & Tosi 2006). However, we can not exclude a priori that systematic errors might be hidden in the calibration of the photometry because we could use only tertiary standards (see Sec. 2.2). Concerning the fraction of binary systems and differential reddening we fine-tuned our synthetic CMDs for different amount of these two quantities (as done in other papers of this series, see for example Donati et al. 2012, 2014a). For binaries, we

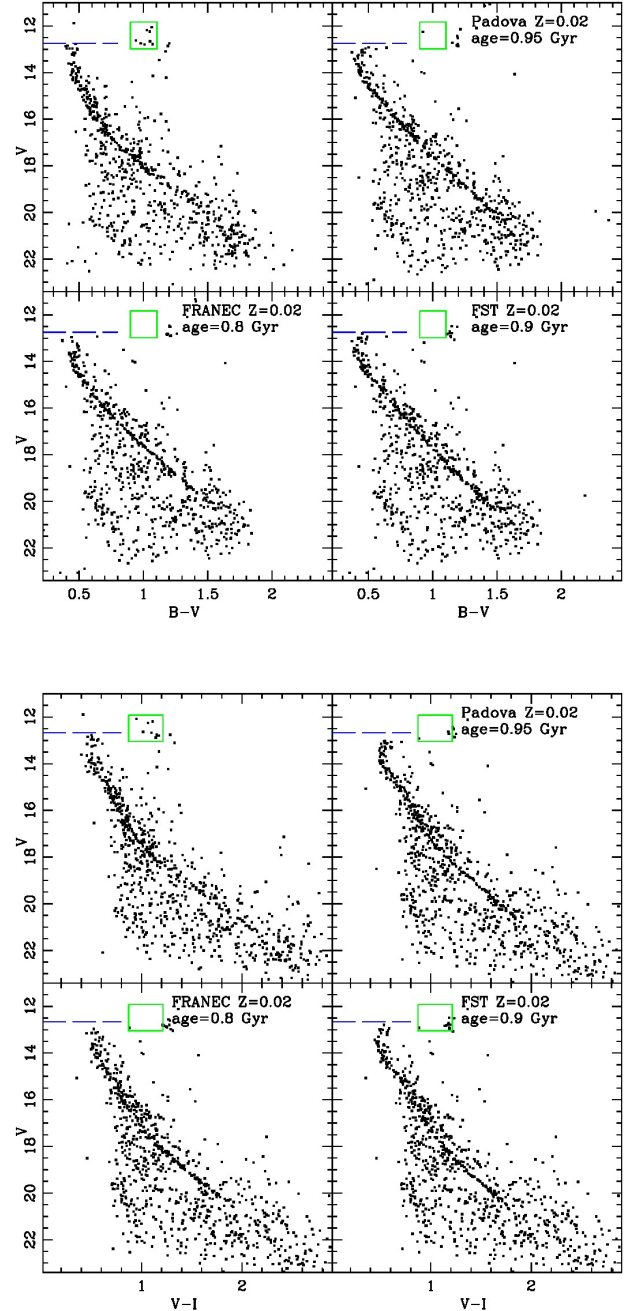


**Figure 8.** In both boxes the upper left CMD is the observational one. The other CMDs are the synthetic ones for the different evolutionary models labelled in each panel and described in this section.

<sup>8</sup> The Padova (Bressan et al. 1993), FRANEC (Dominguez et al. 1999), and FST (Ventura et al. 1998) with  $\eta = 0.2$ . We keep using these relatively old models for sake of homogeneity within the BOCCE sample of clusters.

build synthetic CMDs where the desired percentage of objects is not a single star but objects that have the photometric properties of two randomly picked synthetic stars as they were photometrically unresolved. In the case of differential reddening, the adopted quantity is considered as an upper limit and added as a random positive constant to the mean Galactic reddening. We found that the best estimation for the binary fraction is 35% and for the differential reddening

is 0.08 mag, and kept them fixed for all the following analysis.

Figure 8 shows the comparison between the observational CMD inside 5' from the cluster centre (a good compromise between having enough cluster stars in all evolutionary phases and low field stars contamination) and the best fits obtained with the three sets of tracks. We recall that solar metallicity is assumed in all tests. To better compare data and models we draw the age sensitive indicators (see Sec. 2.4) both in the observed and in the synthetic CMDs.

With the Padova models we found an age of 0.95 Gyr,  $E(B-V) = 0.14$  mag, and distance modulus  $(m-M)_0 = 10.92$  mag. This model can adequately reproduce the luminosity levels of the MSTP and RC. For the latter we obtained a good match of the colour on the  $V, V - I$  plane while in  $V, B - V$  the synthetic clump is too red (about 0.1 mag redder). Especially in the  $V, V - I$ , the model well fit the observed MS down to magnitude  $V \sim 20$  mag.

For the FST models we found the best fit for an age of 0.9 Gyr,  $E(B-V) = 0.15$  mag, and distance modulus  $(m-M)_0 = 11.04$  mag. The colour and magnitude of the MSTP are well reproduced and we found a very good fit to the MS especially in  $V, V - I$  down to magnitude  $V \sim 19$  mag. The luminosity and colour of the RC are perfectly reproduced in the  $V, V - I$  plane while the synthetic RC is slightly redder than observed in the  $V, B - V$  plane.

In the case of the FRANEC models we obtained the best fit for an age of 0.8 Gyr,  $E(B-V) = 0.19$  mag, and distance modulus  $(m-M)_0 = 10.91$  mag. For this set of models we obtained the best fit of the MS down to magnitude  $V \sim 22$  mag, in particular in the  $V, V - I$  plane, while the RC colour is too red in both  $V, B - V$  and  $V, V - I$  synthetic CMDs. As expected, the ages derived from the FRANEC models are lower than those from the other models. This is because the FRANEC tracks do not include overshooting from convective cores, while the other two sets do.

Table 12 shows the cluster parameters we derived, together with the implied Galactocentric distance, height above the Galactic plane, and mass at the MSTO. The typical errors on the cluster parameters are of the order of 0.05 Gyr in age, 0.05 mag in reddening and 0.1 mag in distance modulus as found in other papers of this series. For comparison, literature values range between 0.7 and 1 Gyr for the age, 0.1 and 0.3 mag for the reddening, 10.8 and 12 mag for the distance modulus (see Tab. 1). The age estimates are in good agreement with our analysis while the broad literature range of the other two parameters is likely due to the intrinsic difference of the analysis method and to the different metallicity estimates adopted (usually lower than the solar value we used). In fact, metallicity has a larger impact on reddening and distance modulus than on age, which is less effected.

## 5 DISCUSSION

With the analysis of NGC 2355, both with photometry, to obtain age, distance, and reddening, and with spectroscopy for detailed chemistry, we add another cluster to the homogenous sample of BOCCE clusters.

To put NGC 2355 in the context of other OCs studied, we plot in Figure 9 our results on a compilation of literature

data. We took Table 13 of Yong, Carney, & Friel (2012) as a starting point, but added other clusters analyzed in later papers. Then, to have a more homogenous set, we selected only clusters in the BOCCE sample, either because we derived their distance and age (and often, but not necessarily, the chemical abundances) or their composition (but not age and distance). We ended up with 30 selected clusters, for six of which we adopted literature distance and age while all the others have our BOCCE values; 12 of the 30 clusters have only one spectroscopic analysis, 14 have two, and four have three or more. NGC 2355 falls within the distribution of the other clusters abundances. The information on this sample of OCs (clusters, distance, age, metallicity, and selected elemental ratios, and references for these values) is given in Table 13. No homogenisation has been done, we report results from the original papers.

Classically, OCs have been used to describe the disc metallicity distribution (e.g., Friel 1995; Magrini et al. 2009; Lépine et al. 2011; Andreuzzi et al. 2011; Yong, Carney, & Friel 2012; Heiter et al. 2014, to cite only a few papers). The need of a homogeneous analysis for a large sample of clusters is one of the drivers of the BOCCE project; however, we have not yet reached that goal. Large surveys (e.g., Gaia-ESO, APOGEE, GALAH, see Gilmore et al. 2012; Frinchaboy et al. 2013; De Silva et al. 2015, respectively) targeting also clusters will be fundamental in this respect, but they have not reached yet the “critical mass”. In the meantime, Fig. 10 shows the possibilities and the limits of what can be done with the present samples (see also the discussion in Heiter et al. 2014). In the upper panel we show the metallicity distribution, which displays a negative radial gradient in most of the disc, but a flatter slope in the outer part ( $R_{GC} \gtrsim 12$  kpc)<sup>9</sup>. Lines connect the different metallicities for the same cluster and we see that in some cases the differences exceed 0.1 dex, a reasonable average errorbar for the measures. The radial metallicity distribution of OCs can be interpreted in the light of chemical evolution models (see e.g. Chiappini, Matteucci, & Romano 2001; Magrini et al. 2009; Romano et al. 2010), in which the rapid star formation rate in the inner disc together with the assumption of a different rate of infalling material from the intergalactic medium onto the inner and outer disc, predict a negative metallicity gradient in the inner disc and a flattening in the outer one. However, the issue of the time evolution of the radial abundance gradients is far from being settled unequivocally both from the theoretical (different model prescriptions lead to different scenarios: either a flattening or a steepening of the inner gradient with time) and observational points of view (some authors suggest that the radial metallicity distribution is not a negative gradient but rather a step distribution, see e.g. Twarog, Ashman, & Anthony-Twarog 1997; Lépine et al. 2011). The interpretation becomes even more intriguing when dynamics is considered in galactic chemical evolution models. For example, flat abundance gradients could also be produced when radial mixing is taken into account (e.g., Roškar et al. 2008; Sánchez-Blázquez et al. 2009; Minchev et al. 2011, 2012). Fujii & Baba (2012), using N-body simula-

<sup>9</sup> All  $R_{GC}$  values have been computed using uniformly  $R_{GC,\odot} = 8$  kpc, also for the clusters for which we took distances from literature.

**Table 12.** Cluster parameters derived using different models. Recall that the spectroscopic metallicity we found is slightly lower than solar.

| Model  | age<br>(Gyr) | $Z^a$ | $(m - M)_0$<br>(mag) | $E(B - V)$<br>(mag) | $d_\odot$<br>(kpc) | $R_{GC}^b$<br>(kpc) | $Z$<br>(pc) | $M_{TO}$<br>( $M_\odot$ ) |
|--------|--------------|-------|----------------------|---------------------|--------------------|---------------------|-------------|---------------------------|
| Padova | 0.95         | 0.02  | 10.916               | 0.14                | 1.52               | 9.39                | 312.1       | 2.1                       |
| FST    | 0.9          | 0.02  | 11.035               | 0.15                | 1.61               | 9.47                | 329.7       | 2.2                       |
| FRANEC | 0.8          | 0.02  | 10.911               | 0.19                | 1.52               | 9.39                | 311.4       | 2.2                       |

<sup>a</sup>Metal content of the evolutionary tracks.

<sup>b</sup> $R_\odot = 8$  kpc is used to compute  $R_{GC}$ .

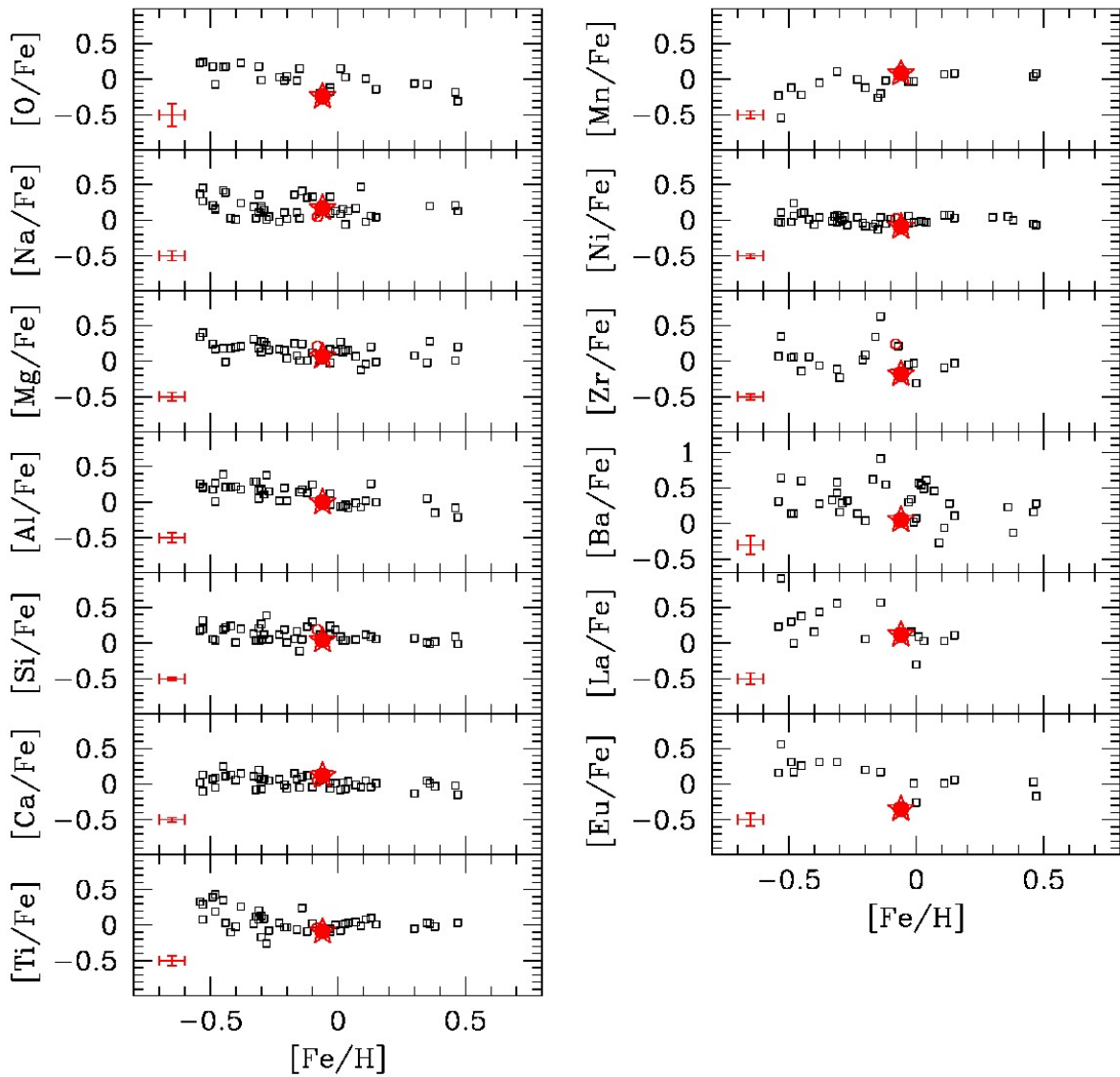


**Figure 9.** Comparison of results for NGC 2355 (indicated by a filled red star) and literature values for open clusters (with multiple results for the same cluster all shown, see text) for the elements in common. The errorbars in each panel are the rms of our values.

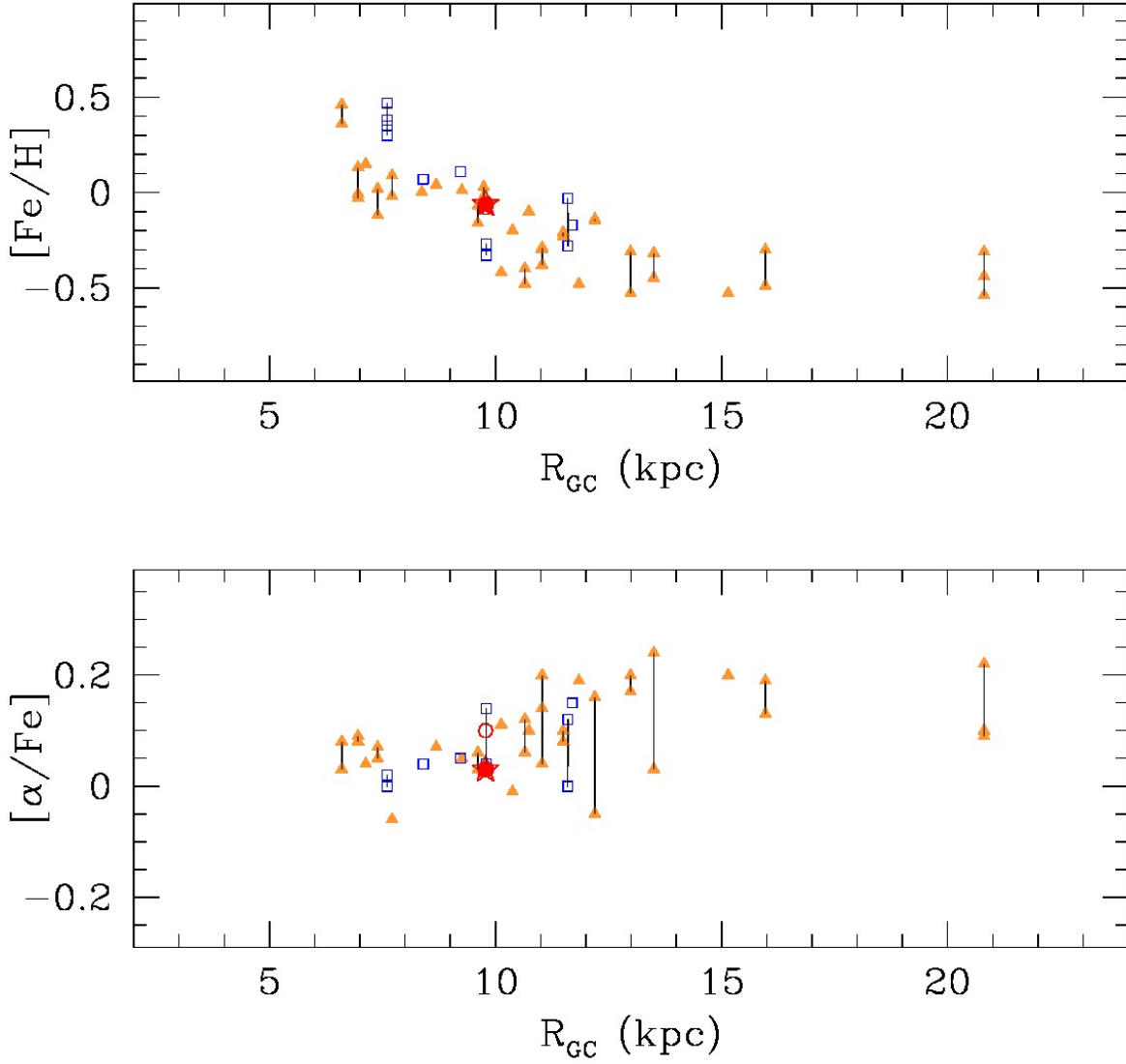


**Figure 10.** Metallicity and  $\alpha$ -elements distributions with Galactocentric distance. Our value for NGC 2355 is indicated by a red star. Orange filled points are clusters with BOCCE age and  $R_{GC}$ , open blue squares clusters with literature age and  $R_{GC}$ . Lines connect different metallicity and  $[\alpha/Fe]$  values for the same cluster. References for the spectroscopic and photometric papers are in Table 13.

tions, found a time-scale of 100Myr for the radial migration of OCs. They demonstrated that in this time a cluster could move 1.5 kpc away from its birth location, a result stressing how important the dynamics can be in interpreting the chemical evolution history of the Galactic disc. However, Haywood et al. (2013), by analyzing FGK stars near the Sun, argue for the lack of a detectable influence of radial migration, at least in the solar neighborhood. Determinations of abundance gradients in the disc at different ages are thus crucial to disentangle among different evolutive scenarios. The Gaia-ESO Survey<sup>10</sup>, with its large spectroscopic legacy (high and intermediate resolution spectra of about

$10^5$  stars in the MW and stars in about 70 OCs) will have an important impact on this side. Furthermore, within the Survey there are ongoing projects focussed on the accurate analysis of clusters orbits (e.g. Jacobson et al. in prep.), following the same approach described in Jílková et al. (2012) in the case of NGC 6791, with the aim to build a comprehensive study of OCs which takes into account homogeneous chemical abundances and kinematics. Gaia<sup>11</sup> will further improve these studies with precise proper motions, helping in determining the impact of dynamics on the MW evolution.

In the lower panel of Fig. 10 we show, for the same sample of OCs, the run of  $\alpha$ -elements with  $R_{GC}$ . The dis-

<sup>10</sup> <http://www.gaia-eso.eu/>

<sup>11</sup> <http://sci.esa.int/gaia/>

**Table 13.** Parameters and elemental ratios for the BOCCCE cluster

| Cluster   | age  | $R_{GC}$ | [Fe/H] | [O/Fe] | [Ne/Fe] | [Mg/Fe] | [Si/Fe] | [Al/Fe] | [Ca/Fe] | [Ti/Fe] | [Mn/Fe] | [Co/Fe]           | [Ni/Fe] | [Ag/Fe] | [Eu/Fe] | [Ba/Fe] | [La/Fe] | [Eu/Fe] | [ $\alpha$ /Fe]           | ref spec                  | ref phot                  |
|-----------|------|----------|--------|--------|---------|---------|---------|---------|---------|---------|---------|-------------------|---------|---------|---------|---------|---------|---------|---------------------------|---------------------------|---------------------------|
| NGC2355   | 0.90 | 9.40     | -0.06  | -0.24  | 0.17    | 0.07    | -0.00   | 0.04    | 0.12    | -0.09   | 0.08    | Age/Rg/HOCC       | -0.09   | -0.18   | 0.05    | 0.12    | -0.35   | 0.03    | here                      | here                      |                           |
| Ba17      | 8.50 | 10.74    | -0.08  | 0.05   | 0.21    | 0.12    | 0.25    | 0.08    | 0.19    | -0.04   | 0.02    | 0.24 <sub>a</sub> | 0.02    | 0.02    | 0.10    | 0.10    | 0.10    | 0.00    | Jacobson+11b              | Tsvetog+97                |                           |
| Ba20      | 5.80 | 15.97    | -0.10  | 0.39   | 0.33    | 0.12    | 0.17    | 0.06    | 0.07    | 0.13    | 0.03    | 0.16              | 0.02    | 0.02    | 0.11    | 0.11    | 0.11    | 0.00    | Bragegilia+06b            | Andreuzzi+11              |                           |
| Ba21      | 2.20 | 12.99    | -0.49  | 0.18   | 0.21    | 0.24    | 0.18    | 0.06    | 0.07    | 0.39    | -0.12   | 0.18              | -0.02   | 0.06    | 0.14    | 0.30    | 0.31    | 0.18    | Yong+05                   | Andreuzzi+11              |                           |
| Ba22      | 2.40 | 13.90    | -0.31  | 0.18   | 0.36    | 0.19    | 0.17    | 0.21    | 0.20    | 0.20    | 0.11    | 0.15              | -0.07   | -0.11   | 0.58    | 0.56    | 0.31    | 0.18    | Yong+12                   | BT06                      |                           |
| Ba29      | 3.70 | 20.81    | -0.45  | 0.17   | 0.45    | 0.18    | 0.20    | 0.32    | 0.20    | 0.29    | 0.29    | 0.19              | -0.10   | -0.14   | 0.60    | 0.38    | 0.26    | 0.24    | Hill&Pasquini+99          | BT06                      |                           |
| Ba31      | 2.90 | 15.15    | -0.53  | 0.24   | 0.27    | 0.40    | 0.22    | 0.20    | 0.18    | -0.08   | -0.54   | 0.25              | 0.11    | 0.35    | 0.64    | 0.91    | 0.56    | 0.20    | Yong+05                   | Bragegilia+08             |                           |
| Ba32      | 5.20 | 11.03    | -0.29  | 0.29   | 0.14    | 0.27    | 0.11    | 0.12    | 0.07    | 0.09    | -0.17   | 0.09              | -0.02   | -0.25   | 0.29    | 0.29    | 0.14    | 0.04    | Friel+10                  | Tosi+07                   |                           |
| Ba39      | 6.30 | 11.50    | -0.30  | -0.01  | 0.20    | 0.15    | 0.19    | 0.27    | 0.11    | 0.18    | 0.26    | -0.05             | 0.15    | -0.04   | -0.06   | 0.28    | 0.44    | 0.31    | 0.20                      | Yong+12                   | Bragegilia+12             |
| Ba66      | 3.80 | 11.85    | -0.23  | 0.03   | -0.02   | 0.17    | 0.02    | 0.12    | 0.02    | 0.07    | 0.03    | 0.00              | -0.09   | -0.04   | -0.02   | 0.14    | 0.10    | 0.09    | 0.08                      | Pancino+10                | Andreuzzi+11              |
| Cr110     | 1.70 | 9.74     | 0.03   | -0.03  | -0.06   | 0.16    | -0.04   | 0.04    | -0.04   | -0.07   | 0.02    | 0.01              | -0.02   | -0.02   | 0.49    | 0.03    | 0.49    | 0.04    | Pancino+10                | BT06                      |                           |
| Cr261     | 6.00 | 6.96     | -0.03  | -0.12  | 0.33    | 0.17    | 0.12    | 0.27    | 0.11    | 0.12    | 0.07    | -0.09             | -0.03   | 0.01    | -0.03   | 0.34    | 0.16    | 0.08    | 0.08                      | Bragegilia+08             | BT06                      |
| NGC1817   | 1.10 | 9.61     | -0.07  | -0.19  | 0.12    | 0.01    | 0.01    | 0.12    | 0.06    | 0.06    | -0.04   | -0.04             | -0.06   | -0.26   | -0.11   | 0.07    | 0.09    | 0.09    | Sestito+07                | Bragegilia+12             |                           |
| NGC2099   | 0.43 | 9.26     | -0.16  | -0.02  | 0.11    | 0.08    | 0.17    | 0.02    | 0.12    | 0.07    | 0.03    | 0.00              | 0.04    | -0.06   | 0.04    | 0.24    | 0.14    | 0.10    | Jacobson+09               | BT06                      |                           |
| NGC2141   | 1.90 | 12.20    | -0.01  | 0.16   | 0.09    | 0.27    | -0.06   | 0.08    | -0.08   | -0.08   | -0.08   | -0.04             | -0.04   | -0.02   | -0.02   | 0.57    | 0.09    | 0.17    | 0.06                      | Pancino+10                | Andreuzzi+11              |
| NGC2223   | 4.80 | 10.13    | -0.15  | 0.15   | 0.43    | 0.24    | 0.24    | 0.24    | 0.24    | 0.24    | 0.24    | -0.20             | 0.04    | -0.02   | -0.02   | 0.34    | 0.16    | 0.08    | 0.08                      | Bragegilia+08             | BT06                      |
| NGC2506   | 1.70 | 10.38    | -0.42  | 0.02   | 0.03    | 0.18    | 0.21    | 0.21    | 0.21    | 0.21    | 0.21    | -0.10             | -0.13   | -0.13   | -0.13   | 0.11    | 0.11    | 0.11    | 0.08                      | LeeBrown+15               | BT06                      |
| NGC2660   | 0.96 | 8.69     | 0.04   | 0.02   | 0.02    | 0.04    | 0.04    | 0.04    | 0.04    | 0.04    | 0.04    | -0.03             | -0.12   | 0.01    | -0.08   | 0.04    | 0.06    | 0.06    | Jacobson+07               | Bragegilia+08             |                           |
| NGC3860   | 0.90 | 7.39     | 0.02   | 0.13   | 0.15    | -0.08   | 0.04    | 0.04    | 0.04    | 0.04    | 0.04    | -0.03             | -0.03   | -0.03   | -0.03   | 0.61    | 0.06    | 0.06    | 0.06                      | Bragegilia+08             | BT06                      |
| NGC6233   | 3.00 | 6.60     | 0.46   | -0.18  | 0.21    | 0.01    | -0.08   | 0.09    | -0.09   | -0.09   | -0.09   | -0.02             | -0.02   | -0.06   | -0.06   | 0.34    | 0.12    | 0.12    | 0.06                      | Bragegilia+08             | BT06                      |
| NGC6619   | 2.99 | 7.71     | -0.09  | 0.47   | -0.12   | -0.07   | -0.12   | -0.07   | -0.02   | -0.01   | -0.01   | -0.01             | -0.01   | -0.06   | -0.06   | 0.91    | 0.57    | 0.57    | 0.17                      | Bragegilia+01             | BT06                      |
| NGC6639   | 1.30 | 8.37     | 0.00   | -0.40  | 0.01    | 0.20    | 0.22    | 0.01    | 0.06    | -0.02   | -0.02   | -0.02             | -0.02   | -0.06   | -0.06   | 0.04    | 0.06    | 0.06    | 0.06                      | LeeBrown+15               | BT06                      |
| Trumpler5 | 4.00 | 10.85    | -0.48  | -0.07  | 0.17    | 0.27    | 0.04    | 0.06    | 0.09    | 0.19    | 0.08    | 0.08              | -0.06   | -0.06   | 0.14    | 0.16    | 0.16    | 0.17    | Monaco+14                 | BT06                      |                           |
| NGC6134   | 0.90 | 7.13     | 0.15   | -0.14  | 0.04    | -0.01   | 0.00    | 0.06    | 0.01    | 0.01    | 0.08    | 0.11              | 0.03    | -0.03   | 0.11    | 0.11    | 0.06    | 0.04    | Carretta+04/Mikolaitis+10 | Ahumada+13                |                           |
| IC4651    | 1.70 | 9.23     | 0.11   | 0.01   | -0.02   | -0.31   | 0.02    | 0.12    | 0.05    | 0.08    | 0.07    | 0.13              | 0.07    | -0.09   | -0.09   | 0.03    | 0.01    | 0.05    | 0.05                      | Carretta+04/Mikolaitis+10 | ATT00                     |
| Me66      | 4.70 | 9.80     | -0.33  | 0.05   | 0.27    | 0.10    | 0.02    | 0.05    | 0.15    | 0.05    | -0.08   | 0.02              | -0.08   | -0.08   | -0.08   | 0.32    | 0.33    | 0.33    | 0.14                      | Sestito+08                | Kassis+97                 |
| NGC2158   | 2.00 | 11.60    | -0.03  | -0.17  | 0.10    | -0.02   | -0.03   | 0.12    | -0.06   | -0.05   | -0.05   | -0.05             | -0.05   | -0.05   | -0.05   | 0.04    | 0.04    | 0.04    | 0.00                      | Carraro+02                | Carraro+14                |
| NGC2324   | 0.63 | 11.70    | -0.17  | 0.36   | 0.20    | -0.28   | -0.01   | 0.01    | 0.02    | -0.01   | -0.01   | -0.01             | -0.01   | -0.01   | -0.01   | 0.12    | 0.12    | 0.12    | 0.00                      | Bragegilia+08             | BT06                      |
| NGC2477   | 1.00 | 8.40     | 0.07   | -0.31  | 0.13    | -0.21   | -0.01   | -0.01   | -0.15   | -0.08   | -0.04   | -0.04             | -0.04   | -0.04   | -0.04   | 0.46    | 0.46    | 0.46    | 0.04                      | Bragegilia+08             | BT06                      |
| NGC6679   | 8.30 | 7.60     | 0.47   | -0.03  | 0.38    | -0.15   | -0.02   | -0.02   | -0.08   | -0.02   | -0.02   | -0.02             | -0.02   | -0.02   | -0.02   | -0.13   | -0.17   | -0.17   | 0.02                      | Carretta+07               | Jeffery+11                |
|           |      |          | 0.35   | -0.07  | -0.02   | 0.05    | 0.01    | 0.01    | 0.08    | -0.03   | -0.03   | -0.03             | -0.03   | -0.03   | -0.03   | 0.02    | 0.02    | 0.02    | 0.02                      | Carretta+06               | Grundahl+08/Bragegilia+12 |
|           |      |          | 0.30   | -0.06  | -0.08   | 0.07    | 0.01    | 0.01    | 0.07    | -0.13   | -0.13   | -0.13             | -0.13   | -0.13   | -0.13   | 0.02    | 0.02    | 0.02    | 0.02                      | Roosgaard+15              |                           |

tribution mirrors that of Yong, Carney, & Friel (2012) (see their Fig. 21), and seems to indicate that inner and outer disc OCs have a different level of  $\alpha$  enrichment, with a difference of 0.10–0.15 dex, again considering clusters within about 12 kpc from the Galactic centre and farther than that. However, when discussing both the distributions shown in Fig. 10, we have to keep in mind that the abundance analysis is not fully homogenous. As an example of the importance of a homogenous analysis, we recall the recent study of Magrini et al. (2015) where four inner disc OCs were studied, also in comparison with field stars analysed in the same way, using the same line lists, reference values, etc. In this way it was possible to highlight subtle differences in their chemical composition, being sure that they were not due to systematic errors, and question their origin within the Galactic disc. Similar, more complete studies will be performed on the complete OCs database of the Gaia-ESO Survey and of other similar surveys.

Finally, Figure 11 shows the run of the abundance ratios  $[\text{Ba}/\text{Fe}]$ ,  $[\text{Y}/\text{Fe}]$ , and  $[\text{La}/\text{Fe}]$  with cluster age; in the figure we use our values for NGC 2355 and three sets of data, taken from papers devoted to the study of neutron capture elements in large samples of clusters; a) D’Orazi et al. (2009); Maiorca et al. (2011); D’Orazi et al. (2012); b) Jacobson & Friel (2013); c) Mishenina et al. (2013, 2015). We took the original values from the papers, without any attempt at homogeneization; we used the BOCCE value for age, if available (but taking the original value would not change the picture). As mentioned in Section 3.4, it is now well established that OCs do exhibit an anticorrelation between the  $[\text{Ba}/\text{Fe}]$  ratios and the clusters’ age. In order to provide a theoretical explanation to this abundance trend, D’Orazi et al. (2009) (and subsequently Maiorca et al. 2011, 2012) suggested that Ba production in low-mass AGB stars ( $M < 1.5 M_{\odot}$ ) should be more efficient than that predicted by standard chemical evolution models, being the  $^{13}\text{C}$  pocket, that is responsible for providing neutrons, larger than previously thought. If this were the case, then all the  $s$ -process elements, and in particular La and Ce (belonging to the same second  $s$ -process peak) should follow the Ba pattern, though at different extent. However, different studies have provided contradictory results: whereas Maiorca et al. (2011) concluded that all the other  $s$ -process elements reflect this increasing trend with decreasing age, D’Orazi et al. (2012), Yong, Carney, & Friel (2012), Mishenina et al. (2013), and very recently Reddy et al. (2015) did not confirm such finding. This is also evident in Figure 11, where Y and La, at variance with Ba, show a quite flat behaviour with the OC age. To draw final conclusions on this issue, larger and very homogeneous samples are needed, especially for clusters younger than roughly 500 Myr; at the moment several possibilities remain open (we refer the reader to D’Orazi et al. 2012 for further discussion on this topic, including non-LTE and activity effects impacting on Ba abundances). It is noteworthy that, since  $s$ -process models cannot account for Ba production without bearing enhancements in the other  $s$ -process species, Mishenina et al. (2015) suggested a different synthesis channel to explain this peculiar trend, the so-called intermediate (*i*)  $n$ -capture mechanism where neutron densities are intermediate between the low densities of the  $s$ -process and the very high values of the  $r$ -process (see Cowan & Rose 1977).

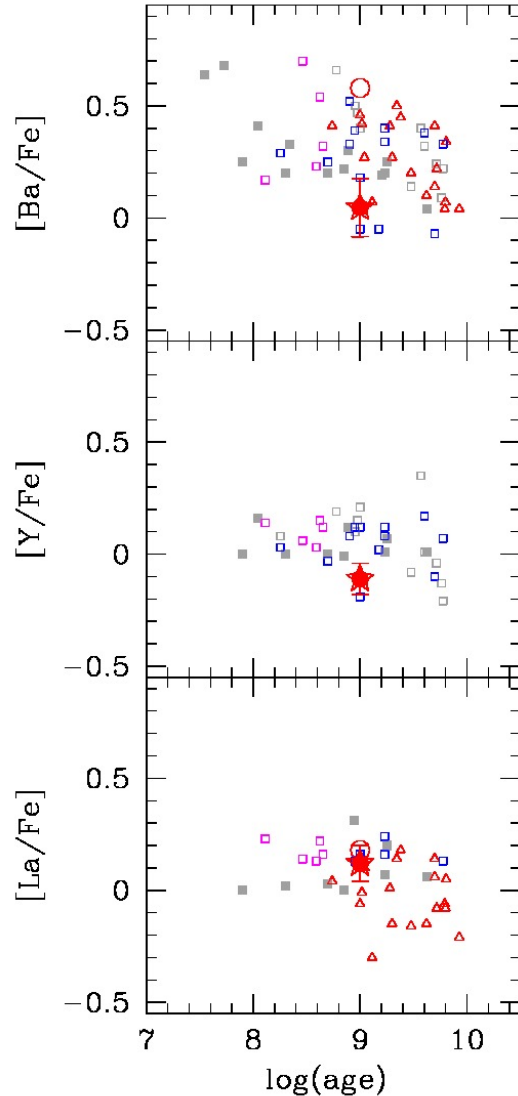


**Figure 11.** Run of  $[\text{Ba}/\text{Fe}]$ ,  $[\text{La}/\text{Fe}]$ , and  $[\text{Y}/\text{Fe}]$  with age obtained by three homogeneous analyses (D’Orazi et al. 2009, 2012, Maiorca et al. 2011: open grey squares for giants, filled grey squares for dwarfs; Jacobson & Friel 2011: open red triangles; Mishenina et al. 2013, 2015: open blue squares; in both cases only giants). For NGC 2355 the value by Jacobson & Friel is indicated by a red empty circles, our by a red star (with errorbars indicating the rms of the measure, see Table 9).

## 6 SUMMARY

We were able to perform a complete analysis of the parameters of NGC 2355, combining precise photometry from LBC@LBT and high-resolution spectroscopy with FIES@NOT.

We obtained observational CMDs two magnitude deeper than literature ones and on a larger FoV. By means of the well tested analysis of cluster parameters with the synthetic CMD technique, we derived age, distance, reddening, differential reddening, and binary fraction with three

different set of tracks (Padova, FST, and FRANEC). We found that NGC 2355 is located at about 1.6 kpc from the Sun. Its Galactic position, towards the anti-centre, is at  $R_{GC} \sim 9.4$  kpc and 300 pc above the plane (assuming  $R_\odot = 8$  kpc). The age is between 0.8 and 0.95 Gyr, depending on the adopted stellar model. The mean Galactic reddening is  $0.14 < E(B-V) < 0.19$  mag, while the estimated differential reddening is about 0.08 mag and the estimated fraction of binaries is about 35%.

The analysis of the high-resolution FIES spectra of three giant stars (belonging to the RC) suggests an almost solar metallicity, with an average  $[\text{Fe}/\text{H}] = -0.06 \pm 0.04$  dex. We derived abundances for O, the light elements Na and Al, the  $\alpha$ -process elements Mg, Si, Ca, Ti (from Ti I and II lines), the Fe-group elements Sc, Cr (from neutral and singly-ionised features), Mn, Ni, Cu, Zn, and for the neutron-capture elements Y, Zr, Ba, La, Ce, Pr, Nd, Eu. When comparing with other OCs at the same metallicity and Galactocentric distance, NGC 2355 falls within the distribution of the other cluster abundances. However, there are some exceptions, especially for neutron capture elements. We discussed possible explanations for these differences, in particular for Ba, which resulted low for the cluster age, compared to expectations based on previous studies. In this case, further investigations are needed to reach a firm conclusion which is, at the moment, constrained only by a limited number of stars.

This analysis represents another step towards the homogeneous tracing of the chemical properties and evolution of the Galactic disc set by the BOCCE project. We are aiming at a database of about 50 OCs to reach statistically significant and accurate results in order to shed a more robust light on the apparent uncertainties that still drive the interpretation of the Galactic disc properties. The achievements of this project, combined with the unprecedented spectroscopic legacy of surveys such as Gaia-ESO or APOGEE and the forthcoming results of the astrometric mission Gaia, will have an important impact on our understanding of the MW.

## ACKNOWLEDGEMENTS

We thank Paolo Montegriffo, whose software for catalogue matching we consistently use for our work. We thank the personnel at LBT and NOT for their help and for taking part of the data. For this paper we used the VizieR catalogue access tool (CDS, Strasbourg, France), WEBDA (originally created by J.-C. Mermilliod and now maintained by E. Paunzen), and NASA's Astrophysics Data System. This research has been partially funded by MIUR and INAF (grants "The Chemical and Dynamical Evolution of the Milky Way and Local Group Galaxies", prot. 2010LY5N2T; grant "Premiale VLT 2012"). Funding for the SDSS and SDSS-II has been provided by the Alfred P. Sloan Foundation, the Participating Institutions, the National Science Foundation, the US Department of Energy, the NASA, the Japanese Monbukagakusho, the Max Planck Society, and the Higher Education Funding Council for England. The SDSS website is <http://www.sdss.org/>. The SDSS is managed by the Astrophysical Research Consortium for the Participating Institutions. The Participating Institutions are the American Museum of Natural History, Astrophysical Institute Pots-

dam, University of Basel, University of Cambridge, Case Western Reserve University, University of Chicago, Drexel University, Fermilab, the Institute for Advanced Study, the Japan Participation Group, Johns Hopkins University, the Joint Institute for Nuclear Astrophysics, the Kavli Institute for Particle Astrophysics and Cosmology, the Korean Scientist Group, the Chinese Academy of Sciences (LAMOST), Los Alamos National Laboratory, the Max-Planck-Institute for Astronomy (MPIA), the Max-Planck-Institute for Astrophysics (MPA), New Mexico State University, Ohio State University, University of Pittsburgh, University of Portsmouth, Princeton University, the United States Naval Observatory, and the University of Washington.

## REFERENCES

Alonso A., Arribas S., Martínez-Roger C., 1999, A&AS, 140, 261  
 Andreuzzi G., Bragaglia A., Tosi M., Marconi G., 2011, MNRAS, 412, 1265  
 De Silva G. M., et al., 2015, MNRAS, 449, 2604  
 Ann H. B., Lee M. G., Chun M. Y., Kim S.-L., Jeon Y.-B., Park B.-G., 1999, JKAS, 32, 7  
 Anthony-Twarog B. J., Twarog B. A., 2000, AJ, 119, 2282  
 Ahumada A.V., Cignoni M., Bragaglia A., Donati P., Tosi M., Marconi G., 2013, MNRAS, 430, 221  
 Bellazzini M., Fusi Pecci F., Messineo M., Monaco L., Rood R. T., 2002, AJ, 123, 1509  
 Boesgaard A. M., Lum M. G., Deliyannis C. P., 2015, ApJ, 799, 202  
 Bragaglia A., Tosi M., 2006, AJ, 131, 1544  
 Bragaglia A., et al., 2001, AJ, 121, 327  
 Bragaglia A., Tosi M., Carretta E., Gratton R. G., Marconi G., Pompei E., 2006a, MNRAS, 366, 1493  
 Bragaglia A., Tosi M., Andreuzzi G., Marconi G., 2006, MNRAS, 368, 1971  
 Bragaglia A., Sestito P., Villanova S., Carretta E., Randich S., Tosi M., 2008, A&A, 480, 79  
 Bragaglia A., Gratton R. G., Carretta E., D'Orazi V., Sneider C., Lucatello S., 2012, A&A, 548, A122  
 Bressan A., Fagotto F., Bertelli G., Chiosi C., 1993, A&AS, 100, 647  
 Brogaard K., et al., 2012, A&A, 543, A106  
 Carraro G., Girardi L., Mariño P., 2002, MNRAS, 332, 705  
 Carraro G., Bresolin F., Villanova S., Matteucci F., Patat F., Romaniello M., 2004, AJ, 128, 1676  
 Carraro G., Villanova S., Demarque P., McSwain M. V., Piotto G., Bedin L. R., 2006, ApJ, 643, 1151  
 Carraro G., de Silva G., Monaco L., Milone A. P., Mateluna R., 2014, A&A, 566, A39  
 Carretta E., Bragaglia A., Gratton R. G., Tosi M., 2004, A&A, 422, 951  
 Carretta E., Bragaglia A., Gratton R. G., Tosi M., 2005, A&A, 441, 131  
 Carretta E., Bragaglia A., Gratton R. G., 2007, A&A, 473, 129  
 Chiappini C., Matteucci F., Romano D., 2001, ApJ, 554, 1044  
 Cignoni M., Tosi M., Bragaglia A., Kalirai J. S., Davis D. S., 2008, MNRAS, 386, 2235

Cignoni M., Beccari G., Bragaglia A., Tosi M., 2011, MNRAS, 416, 1077

Cowan J. J., Rose W. K. 1977, ApJ, 212, 149.

Den Hartog E. A., Lawler J. E., Sneden C., Cowan J. J., 2003, ApJS, 148, 543

Dean J. F., Warren P. R., Cousins A. W. J., 1978, MNRAS, 183, 569

De Silva G. M., Freeman K. C., Asplund M., Bland-Hawthorn J., Bessell M. S., Collet R., 2007, AJ, 133, 1161

Dias W. S., Alessi B. S., Moitinho A., Lépine J. R. D. 2002, A&A, 389, 871

Dias W. S., Monteiro H., Caetano T. C., Oliveira A. F., 2012, A&A, 539, A125

Dominguez I., Chieffi A., Limongi M., Straniero O., 1999, ApJ, 524, 226

Donati P., Bragaglia A., Cignoni M., Cocozza G., Tosi M., 2012, MNRAS, 424, 1132

Donati P., Beccari G., Bragaglia A., Cignoni M., Tosi M., 2014a, MNRAS, 437, 1241

Donati P., et al., 2014b, A&A, 561, A94

Donati P., Cocozza G., Bragaglia A., Pancino E., Cantat-Gaudin T., Carrera R., Tosi M., 2015, MNRAS, 446, 1411

D’Orazi V., Magrini L., Randich S., Galli D., Busso M., Sestito P., 2009, ApJ, 693, L31

D’Orazi V., Biazzo K., Randich S., 2011, A&A, 526, AA103

D’Orazi V., Biazzo K., Desidera S., Covino E., Andrievsky S. M., Gratton R. G., 2012, MNRAS, 423, 2789

D’Orazi V., Campbell S. W., Lugaro M., Lattanzio J. C., Pignatari M., Carretta E., 2013, MNRAS, 433, 366

Ducourant C., et al., 2006, A&A, 448, 1235

Friel E. D., 1995, ARA&A, 33, 381

Friel E. D., Jacobson H. R., Pilachowski C. A., 2005, AJ, 129, 2725

Friel E. D., Jacobson H. R., Pilachowski C. A., 2010, AJ, 139, 1942

Frinchaboy P. M. et al., 2013, ApJ, 777, L1

Fujii M. S., Baba J., 2012, MNRAS, 427, L16

Gilmore G., et al., 2012, Msgr, 147, 25

Gratton R. G., 1988, Rome Obs. Preprint Ser. 2

Gratton R. G., Carretta E., Eriksson K., Gustafsson B., 1999, A&A, 350, 955

Gratton R. G., Carretta E., Claudi R., Lucatello S., Barbieri M., 2003, A&A, 404, 187

Grundahl F., Clausen J. V., Hardis S., Frandsen S., 2008, A&A, 492, 171

Haywood M., Di Matteo P., Lehnert M. D., Katz D., Gómez A., 2013, A&A, 560, A109

Heiter U., Soubiran C., Netopil M., Paunzen E., 2014, A&A, 561, AA93

Hill V., Pasquini L., 1999, A&A, 348, L21

Jacobson H. R., Friel E. D., 2013, AJ, 145, 107

Jacobson H. R., Friel E. D., Pilachowski C. A., 2007, AJ, 134, 1216

Jacobson H. R., Friel E. D., Pilachowski C. A., 2009, AJ, 137, 4753

Jacobson H. R., Friel E. D., Pilachowski C. A., 2011, AJ, 141, 58

Jacobson H. R., Pilachowski C. A., Friel E. D., 2011b, AJ, 142, 59

Jacobson H. R., Friel E. D., 2013, AJ, 145, 107

Jeffery E. J., von Hippel T., DeGennaro S., van Dyk D. A., Stein N., Jefferys W. H., 2011, ApJ, 730, 35

Jílková L., Carraro G., Jungwiert B., Minchev I., 2012, A&A, 541, A64

Kaluzny J., Mazur B., 1991, AcA, 41, 279

Kassis M., Janes K. A., Friel E. D., Phelps R. L., 1997, AJ, 113, 1723

Krone-Martins A., Soubiran C., Ducourant C., Teixeira R., Le Campion J. F., 2010, A&A, 516, A3

Kurucz R., 1993, ATLAS9 Stellar Atmosphere Programs and 2 km/s grid. Kurucz CD-ROM No. 13. Cambridge, Mass.: Smithsonian Astrophysical Observatory, 1993., 13

Landolt A. U. 1992, AJ, 104, 340

Lee-Brown D. B., Anthony-Twarog B. J., Deliyannis C. P., Rich E., Twarog B. A., 2015, AJ, 149, 121

Lépine J. R. D., et al., 2011, MNRAS, 417, 698

Lawler J. E., Bonvallet G., Sneden C., 2001, ApJ, 556, 452

Lawler J. E., Wickliffe M. E., den Hartog E. A., Sneden C., 2001, ApJ, 563, 1075

Magrini L., Sestito P., Randich S., Galli D., 2009, A&A, 494, 95

Magrini L., et al., 2015, arXiv, arXiv:1505.04039

Maiorca E., Randich S., Busso M., Magrini L., Palmerini S., 2011, ApJ, 736, 120

Maiorca E., Magrini L., Busso M., Randich S., Palmerini S., Trippella O., 2012, ApJ, 747, 53

Mc William, A., 1998, AJ, 115, 1640

Mc William A., Wallerstein G., Mottini M., 2013, ApJ, 778, 149

Mermilliod J. C., Mayor M., Udry S., 2008, A&A, 485, 303

Mikolaitis Š., Tautvaišienė G., Gratton R., Bragaglia A., Carretta E., 2010, MNRAS, 407, 1866

Mikolaitis Š., Tautvaišienė G., Gratton R., Bragaglia A., Carretta E., 2011a, MNRAS, 413, 2199

Mikolaitis Š., Tautvaišienė G., Gratton R., Bragaglia A., Carretta E., 2011, MNRAS, 416, 1092

Minchev I., Famaey B., Combes F., Di Matteo P., Mouhcine M., Wozniak H., 2011, A&A, 527, A147

Minchev I., Famaey B., Quillen A. C., Di Matteo P., Combes F., Vlajić M., Erwin P., Bland-Hawthorn J., 2012, A&A, 548, A126

Mishenina T., Korotin S., Carraro G., Kovtyukh V. V., Yegorova I. A., 2013, MNRAS, 433, 1436

Mishenina T., et al., 2015, MNRAS, 446, 3651

Monaco L., et al., 2014, A&A, 564, L6

Oliveira A. F., Monteiro H., Dias W. S., Caetano T. C., 2013, A&A, 557, A14

Origlia L., Valenti E., Rich R. M., Ferraro F. R., 2006, ApJ, 646, 499

Pancino E., Carrera R., Rossetti E., Gallart C., 2010, A&A, 511, A56

Rapaport M., et al., 2001, A&A, 376, 325

Reddy, A. B. S., Giridhar, S., Lambert, D. L. 2015, MNRAS, in press, arXiv:1504.05508

Roškar R., Debattista V. P., Quinn T. R., Stinson G. S., Wadsley J., 2008, ApJ, 684, L79

Romano D., Karakas A. I., Tosi M., Matteucci F., 2010, A&A, 522, A32

Sánchez-Blázquez P., Courte S., Gibson B. K., Brook C. B., 2009, MNRAS, 398, 591

Sestito P., Bragaglia A., Randich S., Pallavicini R., Andrievsky S. M., Korotin S. A., 2008, A&A, 488, 943

Skrutskie M. F., et al., 2006, AJ, 131, 1163

Sneden C. A., 1973, PhD thesis, THE UNIVERSITY OF

TEXAS AT AUSTIN.

Soubiran C., Odenkirchen M., Le Campion J.-F., 2000, *A&A*, 357, 484

Steffen M., 1985, *Astronomy and Astrophysics Supplement*, 59, 403

Stetson P. B. 1987, *PASP*, 99, 191

Stetson P. B. 1994, *PASP*, 106, 250

Stetson P. B., Pancino E., 2008, *PASP*, 120, 1332

Telting J. H., et al., 2014, *AN*, 335, 41

Thygesen A. O. et al., 2014, *A&A*, 572, A108

Tosi M., Greggio L., Marconi G., Focardi P., 1991, *AJ*, 102

Tosi M., Bragaglia A., Cignoni M., 2007, *MNRAS*, 378, 730

Twarog B. A., Ashman K. M., Anthony-Twarog B. J., 1997, *AJ*, 114, 2556

Ventura P., Zeppieri A., Mazzitelli I., DAntona F., 1998, *A&A*, 334, 953

Villanova S., Carraro G., Bresolin F., Patat F., 2005, *AJ*, 130, 652

Yong D., Carney B. W., Teixera de Almeida M. L., 2005, *AJ*, 130, 597

Yong D., Carney B. W., Friel E. D., 2012, *AJ*, 144, 95

This paper has been typeset from a *T<sub>E</sub>X/ L<sup>A</sup>T<sub>E</sub>X* file prepared by the author.